Reports on Progress in Physics

REVIEW

Electron capture in stars

To cite this article: K Langanke *et al* 2021 *Rep. Prog. Phys.* **84** 066301

IOP Publishing Reports on Progress in Physics
Rep. Prog. Phys. **84** (2021) 066301 (35pp) https://doi.org/10.1088/1361-6633/abf207

Review

Electron capture in stars

K Langanke[1,2], G Martínez-Pinedo[1,2,3,*] and R G T Zegers[4,5,6]

[1] GSI Helmholtzzentrum für Schwerionenforschung, D-64291 Darmstadt, Germany
[2] Institut für Kernphysik (Theoriezentrum), Department of Physics, Technische Universität Darmstadt, D-64298 Darmstadt, Germany
[3] Helmholtz Forschungsakademie Hessen für FAIR, GSI Helmholtzzentrum für Schwerionenforschung, D-64291 Darmstadt, Germany
[4] National Superconducting Cyclotron Laboratory, Michigan State University, East Lansing, MI 48824, United States of America
[5] Joint Institute for Nuclear Astrophysics: Center for the Evolution of the Elements, Michigan State University, East Lansing, MI 48824, United States of America
[6] Department of Physics and Astronomy, Michigan State University, East Lansing, MI 48824, United States of America

E-mail: k.langanke@gsi.de, g.martinez@gsi.de and zegers@nscl.msu.edu

Received 3 September 2020, revised 28 February 2021
Accepted for publication 25 March 2021
Published 21 May 2021

Abstract

Electron capture on nuclei plays an essential role in the dynamics of several astrophysical objects, including core-collapse and thermonuclear supernovae, the crust of accreting neutron stars in binary systems and the final core evolution of intermediate-mass stars. In these astrophysical objects, the capture occurs at finite temperatures and densities, at which the electrons form a degenerate relativistic electron gas. The capture rates can be derived from perturbation theory, where allowed nuclear transitions [Gamow–Teller (GT) transitions] dominate, except at the higher temperatures achieved in core-collapse supernovae, where forbidden transitions also contribute significantly to the capture rates. There has been decisive progress in recent years in measuring GT strength distributions using novel experimental techniques based on charge-exchange reactions. These measurements not only provide data for the GT distributions of ground states for many relevant nuclei, but also serve as valuable constraints for nuclear models which are needed to derive the capture rates for the many nuclei for which no data yet exist. In particular, models are needed to evaluate stellar capture rates at finite temperatures, where capture can also occur on nuclei in thermally excited states. There has also been significant progress in recent years in the modeling of stellar capture rates. This has been made possible by advances in nuclear many-body models as well as in computer soft- and hardware. Specifically, to derive reliable capture rates for core-collapse supernovae, a dedicated strategy has been developed based on a hierarchy of nuclear models specifically adapted to the abundant nuclei and astrophysical conditions present under various collapse conditions. In particular, for the challenging conditions where the electron chemical potential and the nuclear Q values are of the same order, large-scale shell-model diagonalization calculations have proved to be an appropriate tool to derive stellar capture rates, often validated by experimental data. Such situations are relevant in the early stage of the core collapse of massive stars, for the nucleosynthesis of thermonuclear supernovae, and for the final evolution of the cores of intermediate-mass stars involving nuclei in the mass range $A \sim 20$–65. This manuscript reviews the experimental and theoretical progress recently

* Author to whom any correspondence should be addressed.
Corresponding editor: Professor Gordon Baym.

achieved in deriving stellar electron capture rates. It also discusses the impact these improved rates have on our understanding of the various astrophysical objects.

Keywords: electron capture, supernova, Gamow–Teller strength, charge-exchange reactions

(Some figures may appear in colour only in the online journal)

1. Introduction

Electron capture is one of the fundamental nuclear processes mediated by the weak interaction. In this reaction, a free proton or one bound inside a nucleus is transformed into a neutron by the capture of an electron, producing an electron neutrino. Electron capture on nuclei plays an important role in various dense astrophysical environments and all three properties which characterize this process (change of the nuclear charge, reduction of the number of electrons, and energy release by neutrinos) have important consequences in these astrophysical environments [1]. Stellar electron captures, however, differ significantly from those which can be studied in the laboratory. In the latter, the decay occurs within an atom (or ion) due to the capture of an electron from the atomic cloud, where electrons in tightly bound orbitals are strongly preferred due to their larger probability density at the nucleus. However, in the high-density, high-temperature environments of stars, the atoms are strongly (for example, in our Sun) or completely ionized (in advanced stellar burning stages or supernovae). Hence, stellar capture rates differ from laboratory rates and are, unfortunately, not yet directly experimentally accessible and therefore have to be modeled.

Supernovae are arguably the most important astrophysical sites in which electron capture on nuclei plays a decisive role. These include the core collapse of massive stars [2–4], the final evolution of the ONeMg cores in intermediate-mass stars [5, 6], the crustal evolution of neutron stars in binaries [7, 8], as well as the nucleosynthesis occurring in thermonuclear (type Ia) supernovae [9, 10]. In all of these scenarios, the densities at which electron capture plays a role are in excess of about 10^9 g cm^{-3} and the finite temperatures range from 10^8 K in electron-capture supernovae to more than 10^{10} K late in the core collapse of massive stars. Under these conditions, electrons are characterized as a relativistic Fermi gas with Fermi energies of MeV to tens of MeV. As a consequence, under these conditions, electron capture can also occur on nuclei that are stable under laboratory conditions [2].

At relatively low electron energies, the capture is dominated by allowed Gamow–Teller (GT) transitions; forbidden transitions contribute at higher densities/temperatures or in exceptional cases [2, 3, 11–13]. This observation has provided the basis for recognizing the importance of electron capture in core-collapse supernova, but has also allowed decisive progress to be achieved in recent years in deriving reliable stellar capture rates. The pioneering work of Bethe, Brown, Applegate, and Lattimer [2] derived capture rates on the basis of a single GT transition that transforms an $f_{7/2}$ proton into an $f_{5/2}$ neutron. This assumption was motivated by the independent particle model (IPM) structure of ^{56}Fe, which is quite abundant during the early collapse phase. The important insight into collapse dynamics achieved in their pioneering work was that electron capture is a very efficient cooling mechanism and that entropy therefore remains low during the entire collapse. As a consequence, the composition of the core is predominantly heavy nuclei rather than being dissociated free nucleons. The challenge of deriving an improved set of stellar capture rates was taken up by Fuller, Fowler, and Newman who, in a series of papers, outlined a formalism for determining stellar capture rates and applied it to the calculation of rate tables for nuclei in the mass range $A = 21$–60 under appropriate temperature and density conditions in the core [3, 14–16]. These derivations were again based on the IPM, but considered experimental data wherever available. Fuller noticed that, within the IPM, GT transitions from pf proton orbitals are Pauli blocked for nuclei with $N \geqslant 40$ for which the pf shell for neutrons is completely filled [17]. Based on this observation, Bruenn derived a parametric description for stellar electron capture rates which assumed vanishing capture rates for all nuclei with neutron numbers $N > 40$ [18]. Although Cooperstein and Wambach pointed out that Pauli blocking could be overcome at high temperatures and by forbidden transitions [11], the Bruenn prescription was the default for electron capture in supernova simulations until the early 2000s (e.g. [1]). On this basis, simulations predicted that, during the advanced collapse phase for densities in excess of 10^{10} g cm^{-3}, electron capture would proceed on free protons rather than on nuclei. Since free protons are significantly less abundant than nuclei during the collapse, electron capture and the associated core cooling was drastically throttled once capture on nuclei was blocked.

During the last two decades, the role played by electron capture in supernova dynamics has been decisively revised. This has been made possible by new theoretical insights, improved models and, not least, by the development of novel experimental techniques to determine nuclear GT strength distributions. This breakthrough was made possible by the observation that strongly forward-peaked cross-sections in charge-exchange reactions mediated by the strong interaction are dominated by the spin–isospin operator needed to derive weak-interaction GT transitions [19, 20]. The pioneering GT measurements were performed at TRIUMF using the (n, p) charge-exchange reaction [21–23]. Despite TRIUMF's moderate energy resolution of about an MeV, these measurements clearly showed that the nuclear GT strength is significantly more fragmented

and also lower in total strength than the predictions of the IPM. These findings were subsequently confirmed by measurements performed at KVI using (d,^{2} He) [24–26], and at the National Superconducting Cyclotron Laboratory (NSCL) by exploiting (t,^{3} He) charge-exchange reactions [27]. With both techniques, experimenters successfully measured GT strength distributions for many pf shell nuclei with an energy resolution that was nearly an order of magnitude better than the resolution available in the pioneering TRIUMF experiments. These measurements became an indispensable constraint for nuclear models, which were developed in parallel with the experimental progress.

Due to the strong energy dependence of phase space, electron capture rates are quite sensitive to the specifics of the fragmentation of the GT strength if the Fermi energies of the electron reservoir and the nuclear Q value are of the same magnitude [12, 28]. This is the case during hydrostatic silicon burning and at the onset of stellar collapse at core densities of up to about 10^{10} g cm^{-3}. Under these conditions, the core mainly consists of nuclei in the Fe–Ni mass range, while sd shell nuclei are also present during silicon burning [29]. The method of choice to describe the properties of these nuclei is the interacting shell model [30]. Due to advances in computational capabilities and progress in software as well as an improved understanding of the decisive ingredients of the residual interaction, diagonalization shell-model calculations became possible for the complete sd shell and for pf shell nuclei at a truncation level that guaranteed sufficiently converged results for the nuclear quantities needed to derive reliable electron capture rates. This, in particular, includes detailed descriptions of the GT strength distributions which, except for a slightly shell-dependent constant factor, reproduced the total GT strength and its fragmentation quite well [31, 32]. This success was first used by Oda and collaborators to derive shell-model electron capture rates for sd shell nuclei [33]. This was followed by the calculation of individual capture rates for nuclei in the mass range $A = 45$–65 based on GT strength distributions derived from large-scale shell-model calculations [12, 34]. Due to the finite temperature of the astrophysical environment, the shell-model calculations also include GT transitions that occur from thermally excited nuclear states. The shell-model rates became the new standard for intermediate-mass nuclei in supernova simulations. It turned out to be quite relevant that the shell-model rates for pf shell nuclei are systematically and significantly smaller than the prior rates based on the IPM [12]. As a consequence, simulations with the shell-model rates showed a noticeably slower deleptonization and resulted in different Fe-core masses at the end of the presupernova phase when the collapse set in [29, 35].

Pauli blocking of the GT strength at the $N = 40$ shell closure exists in the IPM [17], but can be overcome by correlations that move protons or neutrons into the next major shell (the sdg shell) [36]. To describe such cross-shell correlations within the diagonalization shell model usually requires model spaces with dimensions that are not feasible with today's computers. However, such studies exist for ^{76}Se (the intermediate nucleus in the double-beta decay of ^{76}Ge), showing that its GT strength is small, but non-vanishing, even for the ground state [37]. This finding is in good agreement with the experimental determination of the GT strength by the (d,^{2}He) technique [38]. As a consequence, the stellar electron capture rate on ^{76}Se is sizable, showing that the assumption of neglecting capture on nuclei with $N > 40$ is not justified. To derive the stellar capture rate for such nuclei, a hybrid model (HM) had already been proposed and applied prior to the shell model studies of ^{76}Se. This model was based on two steps [36, 39]: first, the crucial cross-shell correlations were studied using the shell-model Monte Carlo (SMMC) approach [40, 41]. These calculations were applied to determine the partial occupation numbers for protons and neutrons in the combined pf–sdg shells and at finite temperatures. In the second step, these partial occupation numbers served as the input for random phase approximation (RPA) calculations of the GT and forbidden strength distributions, and subsequently, the stellar capture rates. The HM was applied to about 200 nuclei in the mass range $A = 65$–110 [28]. The studies clearly implied that Pauli blocking of the GT strength was overcome by cross-shell correlations at the temperature/density conditions at which these nuclei are abundant [28, 42].

Based on the shell-model calculations for the sd and pf shell nuclei, the HM for cross-shell $N = 40$ nuclei, and a parametric study of the heavier nuclei, an electron capture rate table has been derived for core-collapse conditions [13]. The nuclear composition of the core has been assumed to be in nuclear statistical equilibrium (NSE) [43]. When incorporated into supernova simulations, these rates had significant consequences for the collapse dynamics. In particular, the simulations showed that capture on nuclei dominate over capture on free protons during the entire collapse. Furthermore, the dominant capture on nuclei leads to stronger deleptonization of the core and smaller temperatures and entropies, in comparison to the previous belief that capture on nuclei would vanish due to Pauli blocking [28, 42].

As an alternative to the HM, the temperature-dependent quasiparticle RPA (QRPA) model was developed and applied to stellar electron capture for selected nuclei by Dzhioev and co-workers [44]. This approach formally improves upon the HM, since it consistently describes correlations and strength function calculations within the same framework. In contrast to the HM, it restricts correlations to the 2p–2h level which, due to the diagonalization shell-model studies, is not completely sufficient to recover all the cross-shell correlations. This shortcoming is relevant for ground-state strength functions, but diminishes with increasing temperature. Satisfyingly, both distinctly different approaches yield similar capture rates in the density/temperature regimes where nuclei with neutron gaps at $N = 40$ and $N = 50$ matter during the collapse [45].

Electron capture also plays a role in the final fate of the O–Ne–Mg cores of intermediate-mass stars [46, 47] and for the nucleosynthesis responsible for the burning flame during a thermonuclear supernova [48, 49]. In these scenarios, only the sd- and pf-shell nuclei are relevant and hence the respective diagonalization shell-model rates can be applied. For the dynamics of the O–Ne–Mg cores, however, beta decays

are also quite decisive for selected nuclei. The relevant rates can also be calculated quite reliably within the shell model (e.g. [33, 50]). It has been pointed out that electron capture on ^{20}Ne constitutes a very unusual case, as its rate is dominated by a second forbidden ground-state–ground-state transition in the relevant density/temperature regime [51]. As an experimental milestone, this transition has very recently been experimentally determined with quite considerable consequences for our understanding of the fate of intermediate-mass stars [52].

Electron capture on selected nuclei also plays a role during hydrostatic stellar burning or during the slow neutron capture process (the s-process). The description of these capture processes requires a different treatment. In these environments, ions are not completely stripped of electrons, so bound (K-shell) electrons (modified by screening due to the surrounding plasma) are the predominant type captured, but 'free' electrons are also captured from the plasma. We will not review these capture processes in this manuscript, but list a few relevant references for the interested reader. An important example of capture during hydrostatic burning is capture on ^{7}Be, which is a source of high-energy solar neutrinos. The respective solar rate is derived in [53–57]. Electron capture on ^{7}Be is also important in evolved stars, as it affects the abundance of ^{7}Li in red-giant-branch and asymptotic-giant-branch (AGB) stars [58]. During s-process nucleosynthesis, certain pairs of nuclei (such as ^{187}Rh–^{187}Os, ^{205}Tl–^{205}Pb) serve as potential cosmochronometers [59]. These pairs are characterized by very small Q values versus electron captures so that, in the inverse direction, β decay with an electron bound in the ionic K-shell (or higher shells) becomes possible and even dominates the decay. This type of bound-state β decay strongly depends on the degree of ionization and on corrections due to plasma screening, while the competing electron capture process is often modified by contributions due to thermally excited nuclear levels. The formalism used to describe the relevant electron capture, β, and bound-state β-decay rates for the appropriate s-process temperature and density conditions is derived in [60]; detailed rate tables can be found in [61]. The application of these rates to s-process simulations is discussed in [62]. For reviews of s-process nucleosynthesis, the reader is referred to [63, 64].

In this review, we will summarize the theoretical and experimental progress achieved during the last two decades in describing stellar electron capture on nuclei. Section 2 is devoted to the experimental advances describing the various techniques for measuring GT strength distributions. Section 3 starts with some general remarks defining the strategy for deriving the rates under the relevant conditions, followed by some brief discussions of the adopted models and the rates derived within these approaches. In section 4, we summarize the consequences of modern electron capture rates in core-collapse supernovae for the fate of O–Ne–Mg cores in intermediate-mass stars, for the nucleosynthesis in thermonuclear supernovae, and for accreting neutron stars and white dwarfs.

2. Experimental techniques and progress

To accurately estimate the electron-capture rates on nuclei present in stellar environments, it is key to have accurate GT strength distributions from which the electron-capture rates can be derived. Direct information about the GT strength distribution can, in principle, be obtained from β-decay and electron-capture measurements, but this only provides information about transition strengths between the ground states and a limited number of final states. Moreover, since in most astrophysical phenomena, electron capture is most important near the valley of stability and/or on neutron-rich isotopes, the Q value for β^+/EC decay is often negative. This means that direct information is only available for the GT transition strength from the ground state of the mother to the ground state of the daughter derived from β^- decay in the inverse direction, and only if the ground-state-to-ground-state decay is associated with a GT transition. Therefore, an indirect method is needed to gain information about GT strength distributions and to benchmark and guide the development of theoretical models for GT strengths. Charge-exchange reactions [20, 26, 65–67] at intermediate beam energies ($E_{\rm b} \gtrsim 100$ MeV) have served as that indirect method, as it is possible to extract the GT strength distribution at sufficiently high excitation energies to perform detailed assessments of the validity of the theoretical models employed. The remarkable feature of this method is that detailed information about transitions mediated by the weak nuclear force can be extracted from reactions with hadronic probes mediated by the strong nuclear force. The methods and associated experimental techniques are described in this section.

It is important to note that only a limited number of charge-exchange experiments can be carried out and that these experiments only provide data on transitions from the ground state of the mother nucleus. Since, in many astrophysical scenarios, a relatively large number of nuclei play a significant role and, if the stellar environment is at a high temperature, transitions from excited states also play a role, it is rarely possible to rely on the experimental data for GT strength distributions alone. To make accurate estimates of the electron-capture rates in stars, theoretical nuclear models are necessary, which can be tested against charge-exchange data where available. Another important consideration is that electron capture in stars takes place on both stable and unstable nuclei. To obtain information about the latter, charge-exchange experiments with unstable nuclei are needed. As described below, such experiments are challenging; relevant techniques for performing charge-exchange experiments in inverse kinematics are still in development, although good progress has been made over the past decade.

For the purpose of extracting GT strength distributions of relevance for electron capture in stars, charge-exchange experiments in the β^+/EC direction or the (n, p) direction are necessary and are the primary focus of this section. These experiments probe proton–hole and neutron–particle excitations. However, charge-exchange data in the β^- or

(p, n) direction (neutron–hole, proton–particle excitations) are important as well. First, the development of techniques for extracting GT strengths has primarily been developed by using the charge-exchange reaction in the β^- direction, starting with the pioneering work described in [68]. Many detailed studies have been performed using the (^{3}He, t) reaction, benefiting in part from the fact that, for mirror nuclei, the β^+ decay of the neutron-deficient nucleus and the (p, n)-type reaction on the mirror neutron-rich nucleus populate states with the same isospin. This allows detailed comparisons of GT strengths through β decay and charge-exchange reactions [67].

Second, for certain astrophysical phenomena, detailed information is needed about the GT strengths in the β^- direction. Third, by assuming isospin symmetry, information about GT strengths in the β^+/EC direction can sometimes be derived from data in the β^- direction. Finally, the theoretical models used to calculate GT strength distributions in the β^+ direction usually rely on the same parameters for the nuclear interaction as those calculated in the β^- direction. Hence, by comparing the results of models with data from charge-exchange experiments in the β^- direction, additional information about the strengths and weaknesses of those models can be obtained. The summed GT strengths in the β^+ and β^- directions are connected through a sumrule first developed by Ikeda, Fujii and Fujita [69]:

$$S_{\beta^-}(\mathrm{GT}) - S_{\beta^+}(\mathrm{GT}) = 3(N-Z). \tag{1}$$

Although only about 50%–60% of the sum-rule strength is experimentally observed in GT resonance at excitation energies below ∼20 MeV [19, 70], referred to as the 'quenching' phenomenon [20], it allows one to obtain information about the strength in the β^+/EC direction from the measurement in the β^- direction. However, as the electron-capture rates that are derived from the GT strength strongly depend on the strength distribution and not just the magnitude of the strength, measurement of the strength in the β^- direction is of limited use for detailed evaluations of the strength distribution. This is especially true for nuclei with increasing neutron numbers for a fixed atomic number, as S_{β^-} becomes increasingly larger than S_{β^+}. On the other hand, the Ikeda sum rule is a very useful constraint on the total GT strength for the cross-sectional calculation of charged-current (ν_e, e^-) reactions for neutron-rich nuclei [71, 72].

2.1. The extraction of GT strengths from charge-exchange data

The extraction of the GT strength distribution from charge-exchange reaction data at intermediate beam energies is based on the proportionality between the GT transition strength B(GT) for a small linear momentum transfer, $q \approx 0$, expressed through the following relationship [68]:

$$\left[\frac{\mathrm{d}\sigma}{\mathrm{d}\Omega}(q,\omega)\right]_{\mathrm{GT}} = F(q,\omega)\hat{\sigma}B(\mathrm{GT}), \tag{2}$$

in which $\frac{\mathrm{d}\sigma}{\mathrm{d}\Omega}(q,\omega)$ is the measured differential cross-section for a transition associated with an energy transfer $\omega = Q_{\mathrm{gs}} - E_x$ and a linear momentum transfer q. Q_{gs} is the ground-state reaction Q value, which is negative for a transition that requires energy. E_x is the excitation energy of the final nucleus. B(GT) is the GT transition strength and represents the same matrix elements as those probed in β and EC decay transitions between the same initial and final states. The condition that $q = 0$ requires that the cross-section is extracted at, or close to, a center-of-mass scattering angle of zero degrees and that an extrapolation is required based on a calculation to correct for the finite reaction Q value. This extrapolation is represented by the factor $F(q,\omega)$. The factor $\hat{\sigma}$ is the so-called unit cross-section, which depends on the reaction kinematics, the nuclei involved in the interaction, and the properties of the nucleon–nucleon (NN) interaction. In the eikonal approximation [68], these components are factorized:

$$\hat{\sigma} = KN|J^2_{\sigma\tau}|. \tag{3}$$

In this factorization, K is a calculable kinematic factor, N is a distortion factor, and $J_{\sigma\tau}$ is the volume integral of the spin-transfer, isospin-transfer $\sigma\tau$ component of the NN interaction [73]. The distortion factor accounts for the distortion of the incoming (outgoing) particle by the mean field of the target (residual) nucleus and can be estimated by taking the ratio of a distorted-wave impulse or Born approximation calculation to a plane-wave calculation [68]. The strength of the method used to extract GT distributions from charge-exchange data is that the details of the components that make up the unit cross-section do not need to be known, since the unit cross-section is conveniently calibrated by using transitions for which B(GT) is known from β-decay experiments. Once established for one or a few transitions for a given nucleus and charge-exchange reaction, the proportionality can be applied to all transitions identified as being associated with $\Delta L = 0$ and $\Delta S = 1$, except for the extrapolation to $q = 0$ through the factor $F(q,\omega)$ of equation (2). This extrapolation carries a relatively small uncertainty. Calibrations for known transitions from β decay are not always possible. Therefore, mass-dependent parametrizations of the unit cross-sections have been successfully developed for the (p, n)/(n, p) [74] and (^{3}He, t)/(t,^{3} He) [75, 76] reactions, which provide a convenient way to extract the GT strength distributions for such cases.

In order to use equation (2) and extract the GT strength distribution from measured differential cross-sections, one must first identify the contributions to the experimental spectra that are associated with monopoles ($\Delta L = 0$) and spin transfer ($\Delta S = 1$). This is performed by investigating the differential cross-sections as a function of scattering angle, since excitations that are associated with increasing units of angular momentum transfer have angular distributions that peak at a larger scattering angle. Therefore, the ΔL = 0 contribution to the cross-section is extracted through a process called multipole decomposition analysis (MDA) [77], in which the measured differential cross-section of a particular peak or data in an excitation-energy bin is fitted by a linear combination of calculated angular distributions for different units of ΔL. An example for the ^{46}Ti(t,^{3} He) reaction is shown in figure 1. Since the $\Delta L = 0$, $\Delta S = 0$ contribution is almost completely associated with excitation of the isobaric analog state, it does

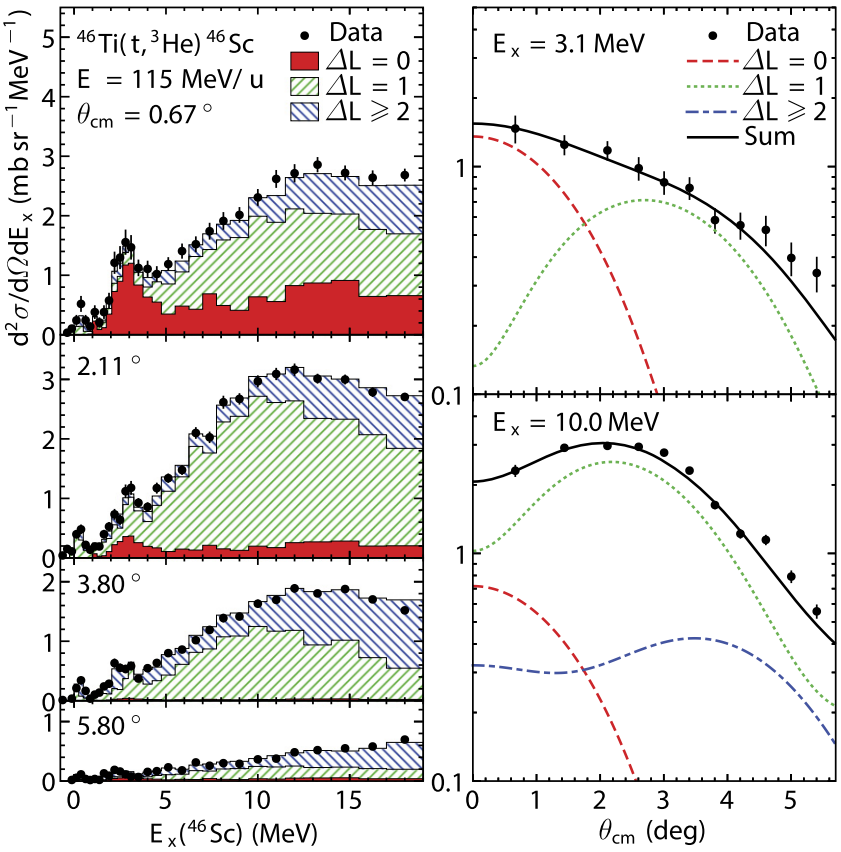

Figure 1. An example of the MDA for the ^{46}Ti(t,^{3} He) reaction at 115 MeV/u. The left-hand side shows differential cross-sections at four scattering angles. The right-hand side shows MDA analyses for two excitation energy bins (at 3.1 MeV and 10 MeV) in ^{46}Sc. The $\Delta L = 0$ ($\Delta L = 1$) contribution is strongest at 3.1 MeV (10.0 MeV). The stacked colored histogram on the left-hand side indicates the contributions from the different angular momentum transfers based on the MDA. Reprinted figure with permission from [78], Copyright (2014) by the American Physical Society.

not contribute to the $\Delta L = 0$ yield for (n, p)-type reactions for nuclei with $N \geqslant Z$, as the isospin of states in the final nucleus always exceeds that of the target. The Fermi sum rule of $S_- - S_+ = (N - Z)$ is nearly fully exhausted by the excitation of the isobaric analog state in the β^-(p, n) direction.

For (n, p)-type reactions, at excitation energies $\gtrsim$10 MeV, contributions to the $\Delta L = 0$ yield arise from excitation of the isovector giant monopole resonances and the isovector spin giant monopole resonance (IVSGMR) [65]. In charge-exchange reactions with beam energies of $\gtrsim$100 MeV, the IVSGMR dominates. Since the angular distribution of the IVSGMR is very similar to that of GT excitation, the two are not easily separable experimentally. Only through a comparison between (n, p) and (t,^{3} He) data it is possible to disentangle the two contributions [79]. Since the transition density for the IV(S)GMR has a node near the nuclear surface, a cancellation occurs for the (n, p) probe that penetrates relatively deeply into the nuclear interior, whereas such a cancellation does not occur for the peripheral (t,^{3} He) reaction [80, 81]. Hence, the excitation of the IV(S)GMR is enhanced for the latter probe. As this comparison between probes is generally unavailable, the extraction of GT strengths for the purpose of estimating electron-capture rates and benchmarking the theory is usually limited to excitation energies of up to about 10 MeV.

Since the GT strengths extracted from the charge-exchange data are calibrated against known weak transition strengths, the uncertainties introduced by the need to extract absolute cross-sections through careful beam intensity normalizations and target thickness measurements are absent. If phenomenological relationships between the unit cross-section and mass number are utilized [75] to determine the unit cross-section, a measurement with a target for which the unit cross-section has been well established is generally included in an experiment, so that a relative normalization can be performed, rather than relying on an absolute cross-sectional measurement that is usually more uncertain. This helps to reduce experimental systematic uncertainties to about 10% [75].

The main remaining uncertainties in the extraction of GT strengths arise from effects that perturb the proportionality of equation (3). It has been shown [27, 82] that the leading cause for the perturbation of the proportionality is the interference between $\Delta L = 0$, $\Delta S = 1$ and $\Delta L = 2$, $\Delta S = 1$ amplitudes that both contribute to $\Delta J = 1$ transitions in which the parity does not change. This interference is mediated by the tensor-τ component of the NN force [20, 73]. The uncertainty introduced by this effect depends on the magnitude of the GT transition strength and was estimated [27] to be $\approx$0.03–0.035 ln(B(GT)), which amounts to an uncertainty of about 20% for B(GT) = 0.01. The results of this study are

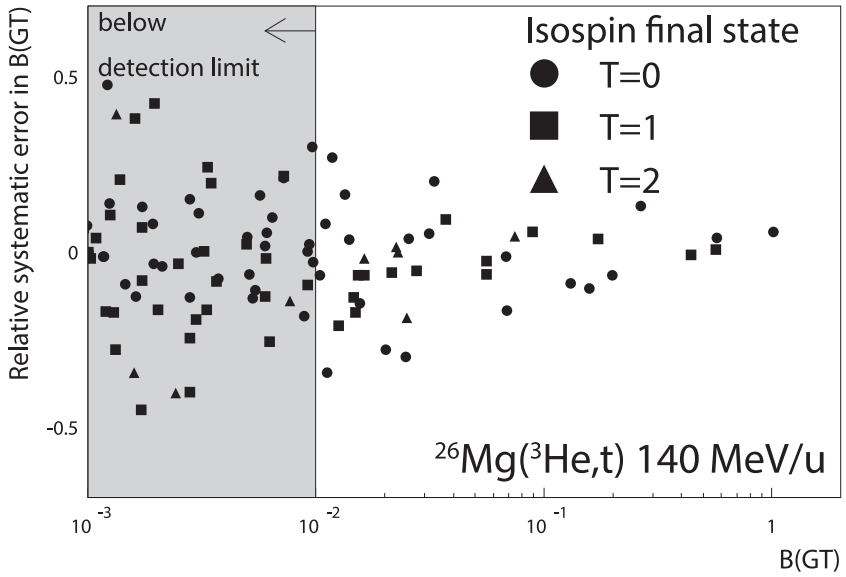

Figure 2. Results from a theoretical study that estimated the magnitude of the uncertainty in the proportionality between GT strength and differential cross-sections for the ^{26}Mg(^{3}He, t) reaction at 140 MeV/u due to the effects of the tensor-τ component of the NN interaction. Transitions to final states in ^{26}Al with isospins of $T = 0, 1$, and 2 are included. The uncertainty increases with decreasing B(GT). The detection limit of 0.01 is indicated. Reprinted figure with permission from [27], Copyright (2006) by the American Physical Society.

shown in figure 2. A B(GT) of 0.01 is close to the detection limit in charge-exchange experiments. It has been shown that this uncertainty estimate is not strongly dependent on the nucleus studied [82]. It is also clear that the systematic deviation fluctuates around 0, and after integrating over many states, the uncertainty in the summed or average transition strength is small.

2.2. Probes

The extraction of GT strengths from charge-exchange reactions in the β^+ direction for the purpose of constraining electron-capture rates has primarily been performed with three probes: the (n, p), (d,^{2}He), and (t,^{3} He) reactions. In this subsection, a brief overview of these three probes and their experimental methods will be provided.

2.2.1. (n, p) *reaction.* Although (n, p) charge-exchange reactions have been performed at a variety of facilities, the pioneering work at TRIUMF has been particularly impactful for the purpose of testing the theoretical models used to estimate electron-capture rates for astrophysical simulations. The nucleon charge-exchange facility at TRIUMF [83, 84] utilized the (p, n) reaction on a ^{7}Li target to produce neutrons of about 200 MeV associated with transitions to the ground and first excited state of ^{7}Be that subsequently impinged on the reaction target of interest. The setup used a segmented target chamber, which allowed for the simultaneous insertion of several targets. Events induced by reactions in different targets were disentangled through the analysis of hit patterns in multi-wire proportional chambers placed in between the targets. Usually, one of the targets was a CH_2 target, so that the well-known ^{1}H(n, p) reaction could be utilized to perform an absolute normalization of the neutron beam intensity. Protons produced in the (n, p) reaction were momentum analyzed using a medium-resolution spectrometer. Measurements at different scattering angles were utilized to determine the differential cross-sections as a function of center-of-mass angles, facilitating the MDA and extraction of GT strength from the proportionality between strength and differential cross-section discussed in section 2.1. A wide variety of experiments were performed for the purpose of extracting GT strengths for astrophysical purposes, primarily using stable nuclei in the pf shell (see e.g. [85–91]). The excitation energy resolutions achieved varied between 750 keV and 2 MeV, depending on the experiment. In figure 3, three examples of the $\Delta L = 0$ contributions extracted for the ^{60,62,64}Ni(n, p) reactions are shown, displaying a concentration of the GT strength at low excitation energies, with a long tail at higher excitation energies.

2.2.2. (d,^{2} He) *reaction.* The (d,^{2} He) reaction has become one of the most powerful probes for studying GT strengths in the β^+ direction. This probe was first developed for the purpose of extracting GT strengths at RIKEN using a 260 MeV deuteron beam [92], followed by the development of this probe at Texas A & M University [93] using a 125 MeV deuteron beam. In these experiments, a resolution of 500–700 keV was achieved, and the beam intensities were limited due to the background from deuteron breakup reactions. The method was perfected in experiments with the Big-Bite spectrometer at the KVI in combination with the EuroSuperNovae detector [94] and using deuteron beams of $\sim$170 MeV. Owing to the use of data signal processing, two-proton coincidence events were selected online, strongly reducing the background from deuteron breakup reactions and making it feasible to run at higher incident beam rates. In addition, the excitation energy resolution was improved to values of typically 150 keV. A recent overview of the (d,^{2} He) program at KVI can be found in reference [26].

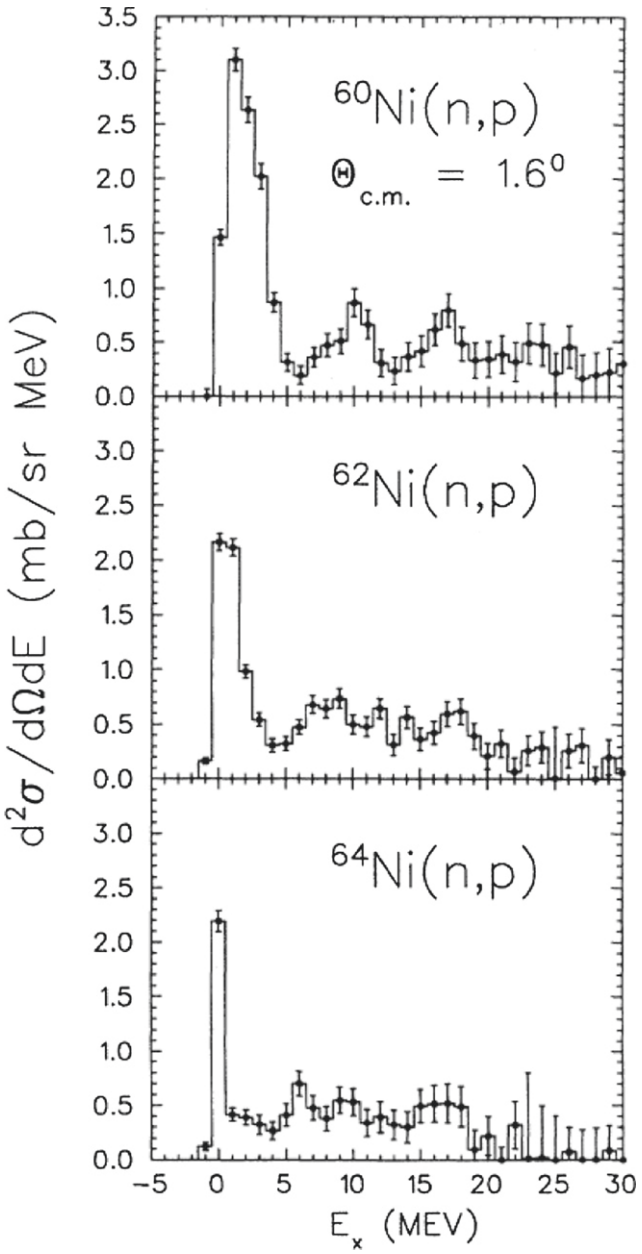

Figure 3. Differential cross-sections associated with $\Delta L = 0$ for the ^{60,62,64}Ni(n, p) reaction at 198 MeV. Reprinted figure with permission from [91], Copyright (1995) by the American Physical Society.

The use of the (d,^{2} He) probe requires that the momentum vectors of the two protons from the unbound ^{2}He must be measured with high accuracy in order to reconstruct the momentum of the ^{2}He particle created in the (d,^{2} He) reaction, as well as the relative energy ϵ between the two protons. On the other hand, the determination of the relative energy makes it possible to enhance the spin-transfer nature of the probe. Since the incident deuterons are primarily in the $^3S_1$ state, a spin-transfer ΔS of 1 is ensured if the outgoing protons couple to the $^1S_0$ state, which can be accomplished by reconstructing the relative energy between the protons and selecting events that have small relative energies (typically smaller than 1 MeV). This removes transitions associated with $\Delta S = 0$ from the spectra and makes it easier to isolate the $\Delta S = 1$ GT transitions.

A variety of (d,^{2} He) experiments have been performed at KVI with the goal of extracting GT strengths to test the theoretical models used to estimate electron-capture rates of interest for astrophysical simulations, see, e.g., references [95, 96–101]. Because of the high resolution achieved, detailed studies of the GT strength distribution could be performed, including studies of nuclei for which it was difficult to obtain the targets, such as ^{50,51}V [95, 97], as shown in figure 4. Clearly, the excellent resolution achieved made it possible to extract very detailed information about the GT strength distribution.

2.2.3. (t,^{3} He) *reaction.* The use of the (t,^{3} He) reaction has the disadvantage that it is complicated to generate tritium beams. Although tritium has been used to produce primary beams (see, e.g., reference [102]), experiments performed for the purpose of extracting GT strength distributions for astrophysical purposes utilized secondary tritium beams. These experiments are performed at NSCL using the S800 spectrometer [103]. A primary ^{16}O beam impinges on a thick beryllium production target to produce a secondary tritium beam of 345 MeV [82]. Because the momentum spread of the secondary beam is large (typically 0.5%), the dispersion-matching technique [104] is utilized to achieve excitation-energy resolutions ranging from 200–350 keV. At present, the beam intensities are limited to about 10^7 particles per second, but with the completion of the Facility for Rare Isotope Beam, the beam intensities will increase significantly.

In addition to the good excitation-energy resolution that can be achieved using the (t,^{3} He) reaction, it has the advantage that the inverse (^{3}He, t) reaction has been studied in great detail and with excellent resolution at comparable beam energies [26, 67, 76]. This makes it possible to utilize the dependence of unit cross-section on mass number determined from (^{3}He, t) data for extracting GT strengths from (t,^{3} He) experiments [27, 75, 76].

As for the (n, p) and (d,^{2} He) reactions, the (t,^{3} He) reaction has been used to study a variety of nuclei to test the theoretical models used in the estimation of electron-capture rates in astrophysical scenarios, e.g., references [78, 105–111]. Since the electron-capture rate is very sensitive to the transitions to the lowest-lying final states in the daughter nucleus, especially at low stellar densities, the (t,^{3} He) probe was combined with the high-resolution detection of γ-rays by a gamma-ray energy tracking in-beam nuclear array [112]. This has made it possible to extract GT transition strengths as low as 0.01 [78], as shown in figure 5 for the ^{46}Ti(t,^{3} He + γ) reaction, for which the B(GT) for the transition to the first 1^+ state at 0.991 MeV could only be determined due to the measurement of the decay γ rays.

In recent years, the focus of the experiments has shifted from nuclei in the pf-shell to nuclei near $N = 50$ [105–107] given their relevance for electron capture rates during the collapse of massive stars (see section 4.1).

2.2.4. (p, n) *reaction and isospin symmetry.* For nuclei with $N > Z$, the GT transition strength in the β^+ direction can also be extracted from (p, n) reactions under the reasonable

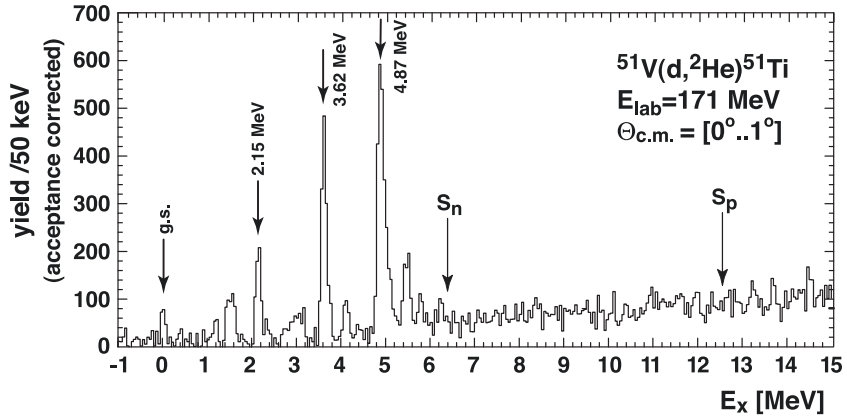

Figure 4. Differential cross-sections at forward scattering angles for the ^{51}V(d,^{2}He) reaction at 170 MeV. Owing to the high resolution, individual transitions are resolved well. Reprinted figure with permission from [95], Copyright (2003) by the American Physical Society.

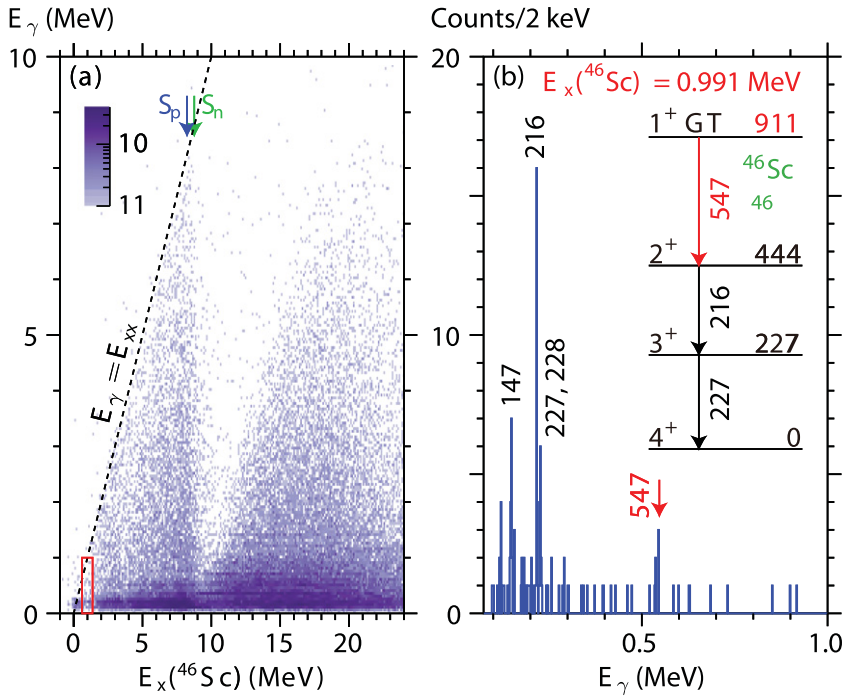

Figure 5. Left: γ energy versus excitation energy for the ^{46}Ti(t,^{3}He + γ) reaction (see also figure 1). Right: by gating on the ^{46}Sc excitation-energy range at around 0.991 MeV, the decay due to a very weak 1^+ state can be identified, which is sufficient for estimating the GT transition strength to this state. Reprinted figure with permission from [78], Copyright (2014) by the American Physical Society.

assumption that isospin-symmetry breaking effects are small. Hence, states with isospin $T_0 + 1$ populated by an (n, p)-type reaction for a nucleus with a ground-state isospin of T_0, have analogs in the (p, n)-type reaction on that same nucleus. By measuring the (p, n)-type reaction and identifying the $T_0 + 1$ states in the spectrum, the GT transition strengths of relevance for estimating electron-capture rates can be extracted. Unfortunately, the excitation of states with higher isospin is suppressed compared to states with lower isospin [113], and the $T_0 + 1$ states appear on a strong background of states with isospin $T_0 - 1$ and T_0, which are also excited in a (p, n)-type reaction on a nucleus with isospin T_0. Still, for nuclei near $N = Z$, GT strengths have been extracted from (p, n) data for the purpose of testing the theoretical models used to estimate electron-capture rates in nuclei [114, 115].

For nuclei with $N = Z$, and assuming isospin symmetry, the GT strength distributions in the β^+ and β^- directions are identical and (p, n)-type measurements can be used to directly obtain the GT strength distribution of relevance for the electron-capture rates. This feature was used to extract the GT strength distribution of ^{56}Ni. The GT strength distribution in ^{56}Cu was extracted by using a novel method to perform a (p, n) experiment in inverse kinematics [116, 117]. The resulting GT strength was the same as the GT strength distribution from ^{56}Ni to ^{56}Co. In this experiment, the excitation-energy spectrum in ^{56}Cu was reconstructed by measuring the recoil neutron from the (p, n) reaction when the ^{56}Ni beam impinged

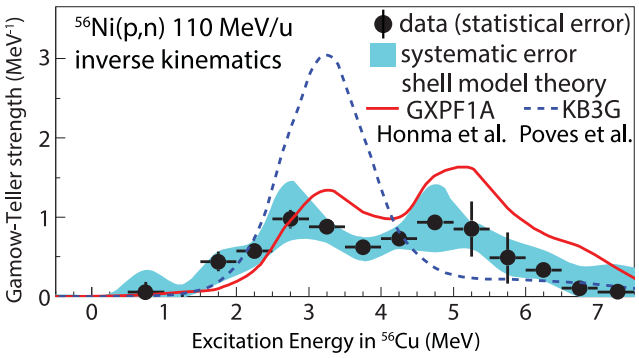

Figure 6. GT strength distribution extracted from the ^{56}Ni(p, n) reaction at 110 MeV/u, performed using inverse kinematics. Two sets of shell-model calculations with different interactions are superimposed. Reprinted figure with permission from [116], Copyright (2011) by the American Physical Society.

on a liquid hydrogen target. Since it is important to measure the reactions under conditions of small linear momentum transfer to maintain the proportionality of equation (2), the relevant recoil neutrons have very low energies and were detected in a neutron-detector array developed especially for that purpose [118]. With this method, it became possible to measure the (p, n) reaction in inverse kinematics for any unstable nucleus. It was recently used to study ^{132}Sn [119].

2.3. (n, p)*-type charge-exchange reactions in unstable isotopes*

Since many of the nuclei that undergo electron capture in stellar environments are unstable, it is important to develop experimental techniques to perform (n, p)-type charge-exchange experiments in inverse kinematics. This poses a significant challenge. A neutron target is not available and all candidate reactions have a light low-energy charged particle as the recoil product, which is not (easily) detectable due to its interaction with the target material. Therefore, in contrast to the (p, n) reaction, the recoil particle is not readily available for the precise reconstruction of the excitation energy and scattering angle of the reaction. If the excitation energy of the residual nucleus after the charge-exchange reaction is less than the nucleon separation energy, a precise measurement of the momentum and scattering angle of the residual can be sufficient to reconstruct the event kinematics. This method was used to extract the small β^+ GT strength distributions from the unstable nuclei ^{12}B and ^{34}Si through the (^{7}Li,^{7} Be) reaction in inverse kinematics [120, 121]. Unfortunately, this probe is very difficult to use when studying the GT strength distributions in unstable nuclei heavier than ^{34}Si. If the excitation energy of the residual exceeds the nucleon separation energy, it is necessary to measure the decay nucleon in addition to measuring the residual. Achieving the necessary energy and angular resolutions to reconstruct the event kinematics becomes challenging because of the strong forward kinematic boost of the laboratory reference frame [120].

Most recently, efforts have been initiated to utilize the (d,^{2} He) reaction in inverse kinematics to study (n, p)-type charge-exchange reactions in unstable isotopes. In such experiments, the rare-isotope beam impinges on an active-target time projection chamber, in which deuteron gas serves both as the target and the detector medium [122]. The tracks from the two protons originating from the unbound ^{2}He particle can be used to reconstruct the momentum of the ^{2}He particle, from which the excitation energy and the scattering angle of the charge-exchange reaction can be determined. The unique two-proton event signature is also very helpful in separating the (d,^{2} He) reaction from other types of reaction that occur in the time projection chamber and that have much higher cross-sections. If successful, the method will be equally powerful for the extraction of GT strengths in the β^+ direction as the (p, n) reaction in inverse kinematics is for the extraction of GT strengths in the β^- direction.

3. Strategy and model for calculating stellar electron capture rates

During their long-lasting lives, stars oppose gravitational contraction using the energy gained from nuclear fusion reactions in their interior. Massive stars develop a sequence of core-burning stages following the CNO cycle, starting by burning hydrogen followed by helium, carbon, neon, oxygen, and then, finally, silicon burning. During this evolution, the density ρ and temperature T in the core gradually increase and reach values in excess of 10^9 g cm^{-3} and 4×10^9 K, respectively, at the onset of collapse. At these high temperatures, nuclear reactions mediated by the strong and electromagnetic force are in equilibrium with their inverse reactions. This situation is called NSE and uniquely determines the nuclear composition for given values of temperature, density and neutronization (usually defined by the proton-to-nucleon ratio Y_e). Once NSE is reached, the star cannot generate energy from nuclear fusion reactions. Hence, the core loses an important source of pressure against gravitational contraction. This situation is reached in the core produced by silicon burning. This core is usually called an iron (Fe) core, because it is made of nuclei in the Fe–Ni mass range, which are favored under the core density and temperature conditions and for a Y_e value only slightly smaller than 0.5. However, the electrons, present in the core to balance the charges of the protons, form a highly degenerate relativistic gas and can balance the gravitational contraction of a stellar mass up to the famous Chandrasekhar limit $M_{Ch} = 1.44(Y_e)^2 M_\odot$, where the solar mass is denoted by $M_\odot$. Once this limiting mass is exceeded by continued silicon burning or, as we will see below, due to electron capture, the electron gas can no longer stabilize the core. The core collapses under its own gravity.

It is important to note that Y_e can be modified by charge-changing reactions which, however, must be mediated by the weak interaction. Such reactions (electron capture, beta decay) are not in equilibrium under the early collapse conditions (since, for example, the neutrinos produced by these processes can leave the star and hence are not available to initiate inverse reactions) and can change the nuclear composition. It is also very important to note that under core-collapse supernova conditions, i.e. at sufficiently high densities, electron capture and beta decay do not balance each other. The reason for this

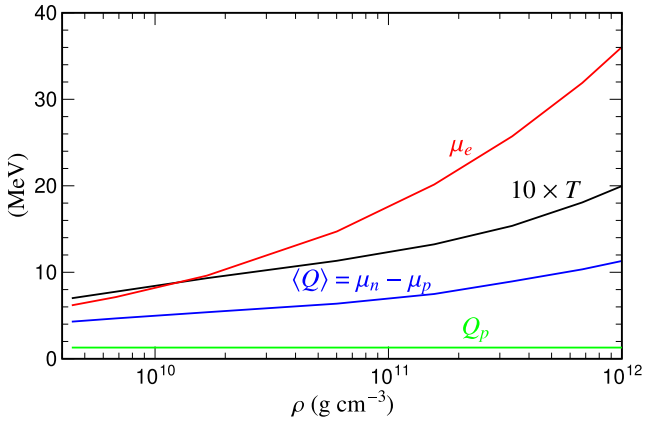

Figure 7. Various energy scales related to electron capture on nuclei and protons as a function of density during the collapse. The plot shows the temperature, T, the chemical potential of electrons, μ_e, the Q value for electron capture on protons (constant) and the average Q value for electron capture on nuclei approximated as the difference in the chemical potential of neutrons and protons. Reprinted from [25], Copyright (2006), with permission from Elsevier.

imbalance lies in the fact that the electron Fermi energy, which scales according to $\rho^{1/3}$, grows noticeably faster than the Q values of the nuclei present in the core (see figure 7). As a consequence, the electron capture rate accelerates, while, conversely, beta decays are throttled due to Pauli blocking of the final electron states. Hence, electron capture wins over beta decay, with three very important consequences. First, electron capture reduces the number of electrons, and hence the degeneracy pressure with which the electron gas can stem the gravitational collapse. Second, the neutrinos produced in the capture process can leave the star nearly unhindered during the early phase of the collapse. They carry away energy which serves as an effective cooling mechanism and keeps the core temperature and entropy low. As consequence of the low entropy, heavy nuclei exist during the entire collapse phase. The situation changes when the collapse reaches densities of the order of 10^{12} g cm^{-3}, where the neutrino diffusion timescale due to coherent scattering on nuclei becomes longer than the collapse time of the core. Neutrinos are then effectively trapped in the core, which collapses as a homologous unit. Third, electron capture reduces Y_e and makes the core composition more neutron-rich. The NSE composition is driven to heavier nuclei with a larger neutron excess (see figure 8). This effect is the reason why nuclei with valence protons and neutrons in different major shells become relevant for electron capture as the collapse progresses, initiating the Pauli unblocking mentioned above.

Electron capture plays an important role in the dynamics of the core collapse of massive stars for core densities between 10^9 g cm^{-3} and 10^{12} g cm^{-3}. Figure 7 shows the evolution of crucial energy scales for this density regime. The most strongly growing quantity is the electron chemical potential μ_e, which increases from 6 MeV to about 40 MeV. As nuclei become increasingly more neutron rich due to continuous electron capture, the average electron capture $\langle Q \rangle$ value of the nuclear composition present at the various stages of collapse grows as well, but this increase is noticeably smaller, from about 4 MeV to 12 MeV. At all stages, the average nuclear $\langle Q \rangle$ value is larger than that for free protons (1.29 MeV). Finally, the temperature in the core also grows during the collapse, from about $T = 0.8$ MeV to $T = 2.0$ MeV. The comparison of these different energy scales allows us to devise a strategy to determine electron capture rates at the needed accuracy for the various stages of collapse.

Figure 9 depicts the consequences which the different behavior of the energy scales has for the electron capture process. We schematically compare the situation in the laboratory with that in the early stage of the collapse, where $\mu_e \approx \langle Q \rangle$, and at an advanced stage with $\mu_e \gg \langle Q \rangle$. In the laboratory, the daughter nucleus must be more bound than the decaying nucleus ($Q < 0$). In our schematic sketch of the GT strength distribution, we indicate that the strongest GT transitions are not accessible in laboratory electron captures at excitation energies of a few MeV. The situation changes completely in the stellar interior, as the capture occurs from a degenerate electron gas. In the early collapse phase (middle diagram), the electron Fermi energy and the nuclear Q value are similar (for example, the Q value of the abundant ^{56}Fe is 4.20 MeV) which makes the calculation of the rate quite sensitive to the reproduction of the small GT strength distribution. An additional complication arises from the fact that the stellar environment has a finite temperature. Hence, capture can also occur from thermally excited nuclear states, which can have different GT strength distributions than the ground state. The nuclear composition at this stage of the collapse is dominated by nuclei in the Fe–Ni range. This is a fortunate situation, as diagonalization shell-model calculations for *pf* shell nuclei are now feasible and have been proven to reproduce GT strength distributions and energy levels quite well. Thus, the diagonalization shell model is the method of choice for determining the capture rates for *pf* shell (and *sd* shell) nuclei.

Due to continuous electron capture, the nuclei abundant in the core composition become more neutron-rich and heavier. The right panel of figure 8 shows the NSE distribution for the conditions reached around the onset of neutrino trapping. The most abundant nuclei correspond to nuclei with valence protons in the *pf* shell, while the valence neutrons occupy orbitals in the *sdg* shell. Hence, the description of cross-shell correlations is the challenge when determining capture rates for these nuclei. We also note that at higher densities, more nuclei contribute to the NSE abundances. This is an effect of the slight increase of core entropy as neutrino-trapping starts and of the decrease of the relative differences of nuclear binding energies as the composition moves to heavier neutron-rich nuclei. The right part of figure 9 describes the energy situation encountered at higher densities in the collapse (a few 10^{10} g cm^{-3} and above). First, the electron chemical potential is now significantly larger than the average nuclear Q-value. For example, the neutron-rich nuclei ^{66}Fe (with $N = 40$) and ^{82}Ge ($N = 50$) have Q-values of 13.8 MeV and 13.0 MeV, respectively. Second, the temperature has grown to about $T = 1$ MeV. At such temperatures, the average nuclear excitation energy, estimated in the Fermi gas model as $E^* = AT^2/8$ is 8.3 MeV for ^{66}Fe and 10.2 MeV for ^{82}Ge and the capture, on average, occurs

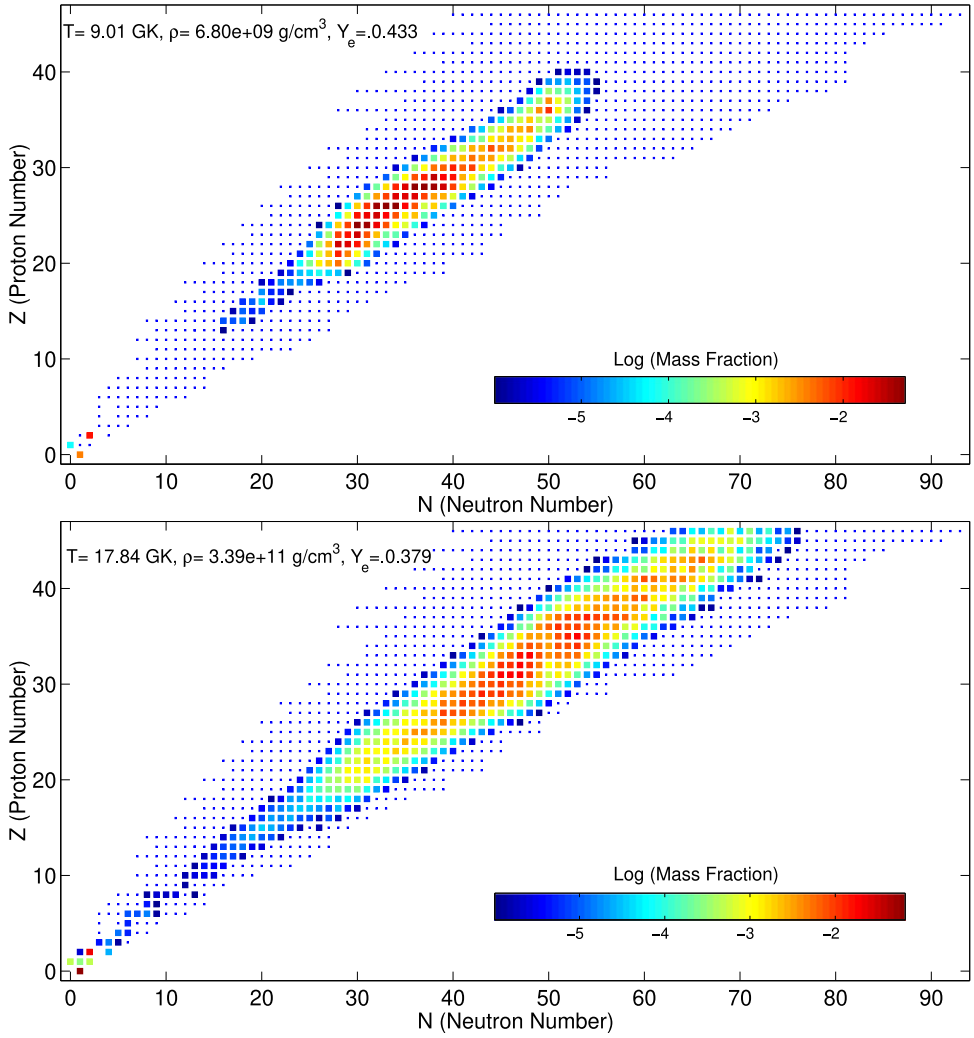

Figure 8. Mass fraction of nuclei in NSE at conditions which resemble the presupernova stage (top) and the neutrino trapping phase (bottom) of core-collapse simulations. Reproduced from [123].

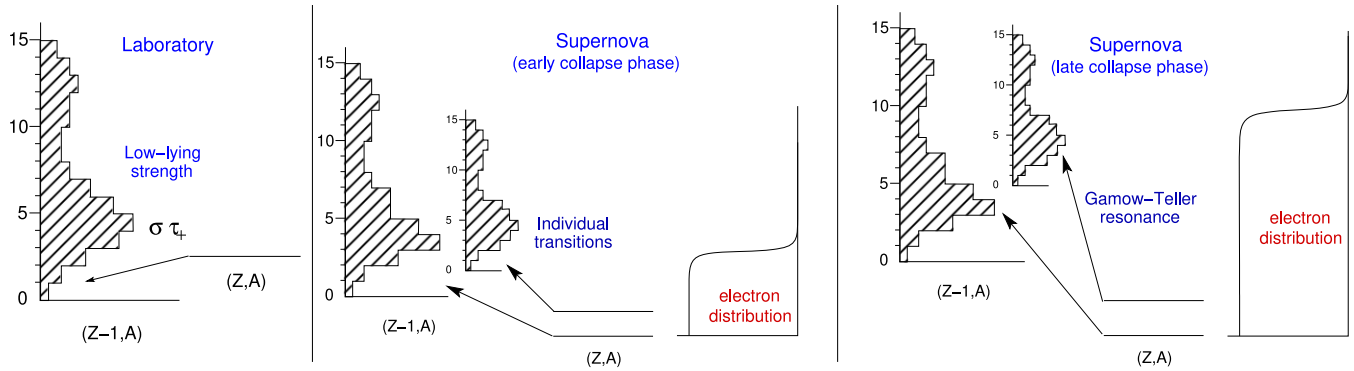

Figure 9. Sketch of electron capture conditions under different conditions: (a) in the laboratory (left), where the electron is captured from an atomic orbital, (b) in the early collapse phase (middle), where the electron is captured from a Fermi–Dirac (FD) distribution with an electron chemical potential on the order of the nuclear Q value, and (c) later in the collapse, at higher densities, where the electrons are captured from an FD distribution with a chemical potential which is noticeably larger than the nuclear Q values. It is important that with increasing core density, the electron chemical potential grows faster than the average nuclear Q value. Electron captures in the star (middle and left) can also proceed from thermally excited states where the temperature and average nuclear excitation energy, respectively, are increasing during the collapse.

from excited states, making it even easier for electron capture to overcome the Q value. Under these conditions, calculations of stellar capture rates for the abundant nuclei on the basis of the diagonalization shell model are not appropriate nor possible. First, diagonalization shell-model studies of nuclear GT strength distributions for the relevant cross-shell nuclei are not yet feasible due to model space restrictions. Moreover, there are simply too many thermally excited nuclear states in the mother nucleus that can contribute to the capture process. However, a detailed reproduction of the GT strength distribution—as required at lower densities where pf shell nuclei dominate—is not needed under conditions of advanced collapse. The fact that the electron Fermi energy and the average nuclear excitation energy are together noticeably larger than the average nuclear Q value makes the capture rate less sensitive to the detailed reproduction of the GT strength distribution. Thus, it suffices if the total GT strength and its centroid are well described, which is possible within the RPA. Second, due to the exponential increase of the level density with excitation energy, there will be many states that contribute to the capture, so some averaging is expected over the GT strength functions. However, there are two further demands which have to be considered. The Pauli unblocking of the GT strength requires the consideration of multi-particle–multi-hole correlations. These correlations are not expected to be the same at the higher excitation energies as they are for the ground state. A many-body method which accounts for both of these effects is the SMMC approach, which allows the calculation of average nuclear properties at finite temperatures considering all many-body correlations in unprecedentedly large model spaces [41]. Hence, an HM that combines partial proton and neutron occupation numbers determined within the SMMC with RPA calculations of the GT and forbidden strength distributions was proposed to calculate stellar electron capture rates for heavy nuclei [39] (see section 3.2). An alternative method to the HM is the temperature-dependent quasiparticle RPA (TQRPA) approach, which treats the ground state and thermally excited states consistently on the level of 2p–2h correlations [44]. This approach has also been used to describe astrophysically-important neutrino-nucleus reactions at finite temperatures [124, 125] (for a review on this subject see [72]).

3.1. Capture rates for nuclei with $A < 65$

The method of choice for determining electron capture and beta decay rates for medium-mass nuclei is the diagonalization shell model. As the shell model allows for the description of individual states and their properties within the chosen model space, the stellar electron capture rate can be determined on the basis of the state-by-state formalism from states in the parent nucleus at energy $E_{\rm i}$ to final states in the daughter nucleus at $E_{\rm f}$. This formalism explicitly considers that the stellar interior has a finite temperature, T. Thus, beta decays and electron captures can occur from excited nuclear levels, where the thermal nuclear ensemble is described by a Boltzmann distribution. Beta decay λ_β and electron capture rates $\lambda_{\rm ec}$ can be derived from perturbation theory and the respective formulas and derivations are presented in [14, 34]. Analytical approximations are provided in [51]. In the derivation of the weak-interaction rates, only GT transitions are included (with an important exception for ^{20}Ne, as discussed below).

3.1.1. pf shell nuclei. The first derivation of stellar weak interaction rates for the pf-shell nuclei relevant to core-collapse supernovae was presented in reference [12]. The calculations are based on diagonalization shell-model calculations considering either all correlations in the complete pf shell or at a truncation level which basically guaranteed convergence of the low-energy spectra and the GT strength distributions, which are the essential quantities used to calculate electron capture and beta decay rates. The GT strength functions were determined using the Lanczos method. Hence, this method represents the strengths of individual states at low energies, while at moderate excitation energies, the GT strength is not completely converged and gives the average value for a rather small energy interval. We note that the shell model generally gives a good account of nuclear properties in the pf shell if appropriate residual interactions, including monopole corrections, are used (see reference [30] and references therein). Reference [32] presented detailed studies of the GT strength distributions and validated the method by comparison to the charge-exchange data available at that time. In fact, good agreement with the data was found, if the shell-model GT distributions were reduced by a constant factor $(0.74)^2$ [126, 127]. The origin of this renormalization (often called quenching of the GT strength) is caused by the fact that shell-model calculations performed within a single shell lack short-range correlations which shift the GT strength to significantly higher energies [128, 129]. Modern many-body techniques, which are able to account for these short-range correlations and include the coupling of the weak force to two nucleons (the so-called two-body currents), indeed recover most of the GT renormalization [130].

Figure 10 compares the shell model GT_+ strength distributions with the experimental data derived from (n, p) charge-exchange reactions and the energy position at which the Fuller, Fowler and Newman (FFN) rates [3] assumed the total GT_+ strength to reside. The fragmentation of the GT strength is quite obvious. It is even more visible in the high-resolution data determined by the (d,^{2} He) and (t,^{3} He) techniques, e.g., see the data for ^{51}V(d,^{2} He) in figure 4. The data for nickel isotopes showed that the KB3 residual interaction, used in references [12, 32], had some shortcomings in describing low-energy details of the GT strength function [131]. These are better reproduced using an alternative residual interaction (GXPF1J [132]) (see figure 6).

Figure 11 compares the electron capture rates calculated for all pf shell nuclei, for which experimental GT_+ distributions have been measured, with the predictions from the shell model on the basis of two residual interactions (KB3G [133] and GXFP1A [134]). The chosen astrophysical conditions correspond to the presupernova stage of the collapse, during which, the pf shell nuclei dominate the abundance distribution. The GXPF1A rates give a nearly perfect reproduction, except for ^{45}Sc. The KB3G rates are slightly worse than those based on the GXPF1A interaction, but still very good, except for ^{45}Sc

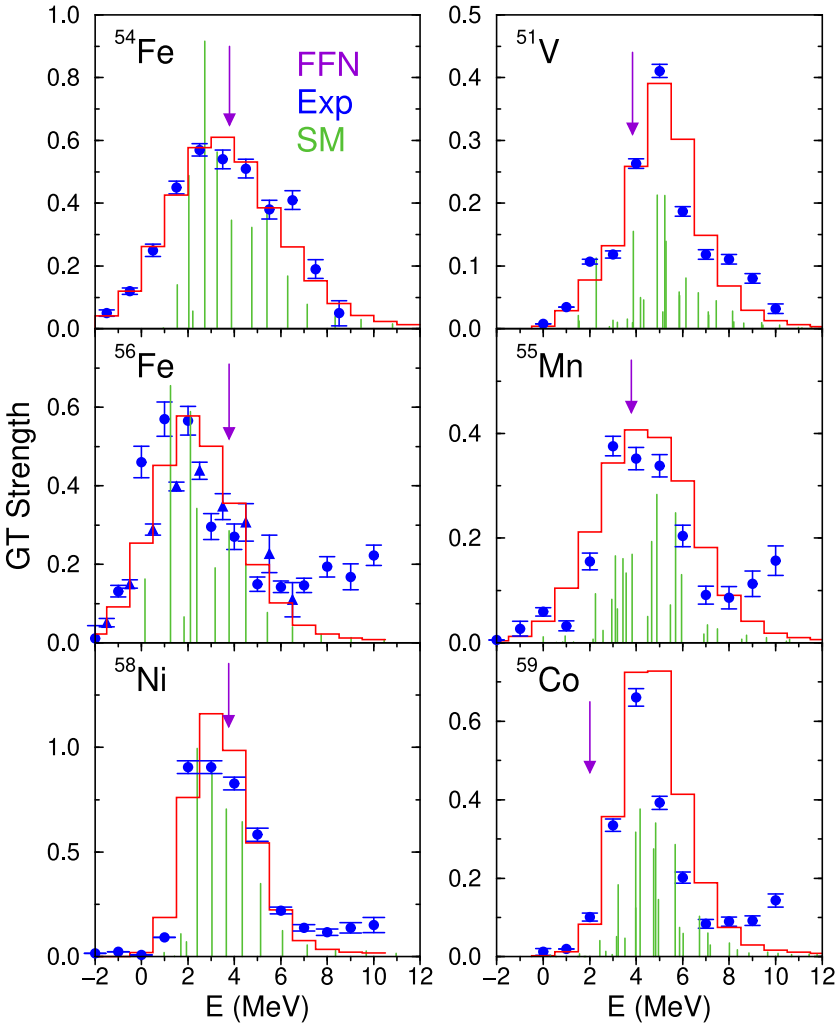

Figure 10. Comparison of experimental and shell-model GT strength distributions for several pf shell nuclei. The data are derived from (n, p) charge-exchange experiments [87, 89, 90]. The shell model results are given as histograms and folded with the experimental energy resolution. The energies at which the FFN evaluation placed the GT strengths are shown as arrows. Reprinted figure with permission from [28], Copyright (2003) by the American Physical Society.

and ^{64}Zn. On the other hand, the rates based on the QRPA calculations, with their restricted account of correlations, can deviate from the data and shell model rates by a factor of up to ten for light pf nuclei, although for the heavier pf shell nuclei, the rates based on the QRPA calculations are reasonable at this stellar density.

The rates presented in figure 11 have been calculated solely from the ground-state GT distribution. This assumes that the GT distributions of excited mother states are the same as for the ground state, shifted only by the respective excitation energy. This assumption often is called Brink–Axel hypothesis [135, 136]. It cannot be strictly valid, as it does not allow for de-excitations. As we will see below, it is also inappropriate for nuclei at shell closures. Reference [137] discusses the validation of this hypothesis. A modification of the Brink–Axel hypothesis for high temperatures is proposed in [138]. A novel method for calculating electron capture rates for excited nuclear states based on the projected shell model was proposed in [139].

Reference [12] calculated stellar beta decay and electron capture rates for more than 100 pf shell nuclei in the mass range $A = 45$–64. These calculations approximated the state-by-state formalism discussed above by explicitly considering the low-energy states and their GT distributions. These contributions were supplemented by the considerations of 'back-resonances'. These are GT transitions calculated for the inverse reaction and then inverted by the detailed balance principle [3, 15]. The calculated energies and GT transition strengths were replaced by experimental data whenever available. A detailed table of the weak interaction rates for the individual nuclei and for a fine grid of astrophysical conditions under which the pf shell nuclei are relevant have been published in [34]. The rate table is publicly available and is incorporated in several leading supernova codes. A procedure for interpolating between the grid points in temperature, density, and Y_e value is discussed in [34], based on the work of [16].

Figure 12 compares the shell model and FFN electron capture rates for several nuclei. The chosen nuclei represent the most abundant even–even, odd–A and odd–odd nuclei for electron capture, as identified by simulations on the basis of the FFN rates under the respective astrophysical conditions

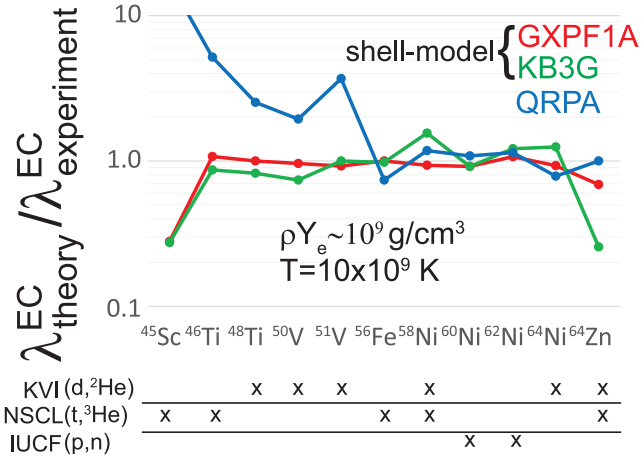

Figure 11. Comparison of electron capture rates for *pf* shell nuclei calculated from experimentally derived GT_+ distributions and from shell-model calculations with two different residual interactions and within the QRPA approach. The astrophysical conditions represent a situation in which *pf* shell nuclei dominate the core composition. The rates presented are originally from [115] and used existing data from (d,^{2} He), (t,^{3} He), and (p, n) experiments, as discussed in section 2. For the purpose of this review, they are supplemented with later results from the (t,^{3} He) reactions in ^{45}Sc [108], ^{46}Ti [78], and ^{56}Fe [109].

during early collapse (the presupernova phase). The shell-model rates are systematically smaller than the FFN rates, with quite significant consequences for the presupernova evolution, as discussed below. The reason for these differences is mainly due to the treatment of nuclear pairing, which was empirically considered in the FFN calculations. This leads, in particular, to the drastic changes observed for odd–odd nuclei. The shell-model rates also considered experimental data which were not available at the time when the FFN rates were derived. The differences between the FFN and shell-model beta decay rates are smaller than for electron capture and do not show a systematic trend [12, 141].

3.1.2. sd shell nuclei. Beta decays and electron capture on *sd* shell nuclei (mass numbers $A = 17$–39) can occur during silicon burning in massive stars [29]. The processes are, however, of essential importance for the fate of the O–Ne–Mg core which develops at the end of hydrostatic burning in intermediate-mass stars. This was the motivation for Oda *et al* [33] to derive stellar beta decay and electron capture rates for *sd* shell nuclei covering the relevant astrophysical conditions (temperatures of 10^8 to 10^9 K and densities of 10^8 to 10^{10} g cm^{-3}). The rate evaluations used the state-by-state formalism defined above. The spectra of the nuclei and the respective GT strength distributions for the ground and excited states were determined by diagonalization in the *sd* shell using the Brown-Wildenthal universal sd-shell (USD) interaction [31, 142], which had been previously proven to give a fairly reliable account of nuclear properties for *sd* shell nuclei. Similarly to the nuclei in the *pf* shell, the GT strength distributions were renormalized by a constant factor. The rates have been made available in tabular form for a grid of temperature–density–Y_e points.

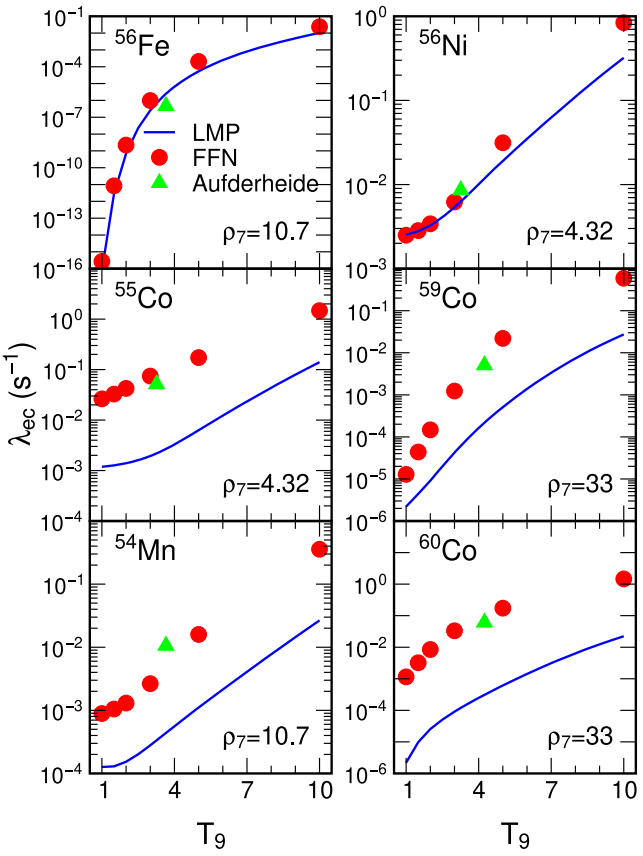

Figure 12. Comparison of the FFN and shell-model rates for selected nuclei as function of temperature (in 10^9 K) and at densities (in 10^7 g cm^{-3}) at which the nuclei are relevant to the capture process in simulations which used the FFN rates. The triangles refer to shell-model estimates derived on the basis of rather strong truncations [140]. Reprinted figure with permission from [28], Copyright (2003) by the American Physical Society.

More recently, an updated rate table was published by Suzuki, based on the USDB residual interaction [143] (a modified version of the USD interaction) and additional experimental information [50]. These modern shell-model rates do not differ by too much from those of reference [33]. However, they are given for a finer mesh of temperature and density. This finer grid is particularly required for the study of the core evolution of stars in the mass regime 8–10$M_\odot$. Of particular importance are the pairs of nuclei ^{23}Ne–^{23}Na, ^{25}Na–^{25}Mg, and potentially ^{27}Mg–^{27}Al, which have Q values versus electron capture that are reached during core contraction at densities of around 10^9 g cm^{-3}. As the environment also has a finite temperature on the order of 10^8 to 10^9 K, which smears the electron's chemical potential and implies the presence of thermally excited states, it is possible that both electron capture and beta decay occur between these pairs of nuclei. The neutrinos produced in both electron capture and beta decay carry energy away, making this URCA process (i.e. electron captures and beta decays between the same pair of nuclei) an efficient cooling mechanism. The operation of the URCA process is restricted to a relatively narrow density range, requiring the knowledge of weak interaction rates on rather fine density–temperature grids. Such rates

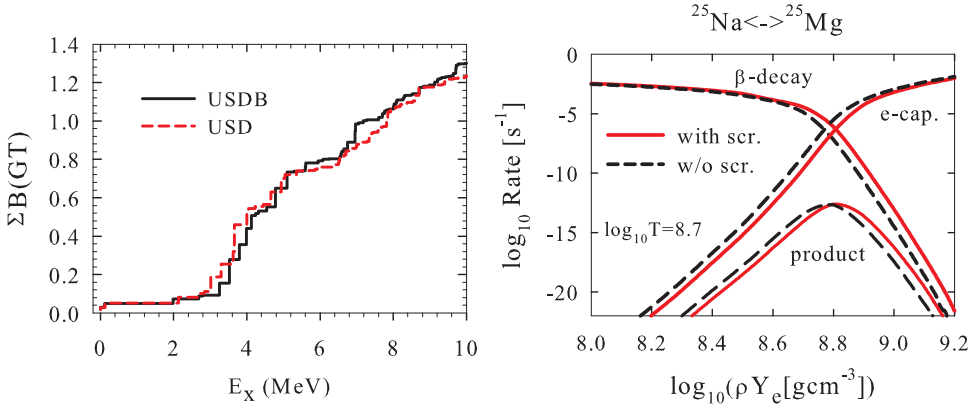

Figure 13. (Left) cumulative GT strength of ^{25}Mg calculated in *sd* shell-model studies for two different interactions. The ground-state strength is experimentally known. (Right) beta decay and electron capture rates for the URCA pair ^{25}Na and ^{25}Mg as function of density and a specific temperature. The curve labeled 'product' is given by the product of the two rates and identifies the density at which the URCA pair operates most efficiently. The rates are given with and without screening corrections. Reproduced from [50].

have been provided in [50, 144]. Figure 13 compares the GT$_+$ strength for the ^{25}Mg ground state as calculated using the USD [33] and USDB [50] interactions. The transition to the ^{25}Na ground state is known experimentally. We note the rather close agreement between the two calculations. Figure 13 shows the beta decay and electron capture rates calculated on the basis of the *sd* shell model. With increasing density, the electron chemical potential grows, which reduces the beta decay rates due to Pauli final state blocking and increases the electron capture rates. At an URCA density of $\log(\rho Y_e[\mathrm{g\ cm^{-3}}]) = 8.81$, both rates match. The product of beta decay and electron capture rates indicates the density range at which the URCA pair operates. Screening effects induced by the astrophysical environment shift the URCA density to slightly larger values (see below).

While the URCA pairs cool the core, electron capture on the two abundant nuclei ^{24}Mg ($Q = 6.03$ MeV) and ^{20}Ne ($Q = 7.54$ MeV) heat it. (The third abundant nucleus, ^{16}O, has such a high Q-value that electron capture does not occur at the densities achieved during the evolution of the ONeMg core). Electron captures on these nuclei start when the core density is large enough for the electron chemical potential to overcome the respective Q value. (Due to its lower Q value, this occurs first on ^{24}Mg.) At these densities, the electron captures on the daughter nuclei ^{24}Na and ^{20}F, respectively, occur with noticeably larger capture rates, as the odd–odd daughter nuclei have significantly smaller Q-values against electron capture due to pairing effects. As $\mu_e > Q$, the capture often leads to excited states in the final nuclei ^{24}Ne and ^{20}O, which de-excite via gamma emission that heats the environment.

The electron capture rates for ^{20}Ne and ^{24}Mg and their daughters have been determined on the basis of shell-model calculations by Takahara *et al* [47] and Oda *et al* [33]. These rates were used as the default values until recently in studies of the core evolution of intermediate-mass stars. The ^{24}Mg capture rate was updated in reference [51] using experimental data which became available in the meantime leading to rather small modifications. This is different for the electron capture rate on ^{20}Ne, which can be considered a milestone and an exception. First, reference [51] showed that all the relevant GT contributions to the rate could be derived from experiments by using data from (p, n) charge-exchange measurements [145] (applying isospin symmetry) and from beta decays of ^{20}F (see figure 14). Furthermore, the authors noticed that, due to the relatively low temperatures of a few 10^8 K, the (at the time, unknown) ^{20}Ne–^{20}F ground-state-to-ground-state transition might contribute to the capture rate at the relevant densities, despite the fact that it is highly suppressed due to angular momentum mismatch. The strength of this second forbidden transition has recently been measured in a dedicated experiment at the IGISOL facility in Jyväskylä [52, 146], and it was found to be large enough to increase the ^{20}Ne capture rate by several orders of magnitude, as shown in figure 14. We emphasize that the electron capture rate on ^{20}Ne in the temperature–density range important for intermediate-mass stars is now completely determined by experiment. This is quite an achievement and shows the great opportunities offered by modern radioactive ion beam (RIB) facilities. That a second forbidden transition essentially contributes to an astrophysical electron capture rate is exceptional, and is the result of the low temperature of the environment and the peculiar structure of ^{20}Ne. In core-collapse supernovae, the temperatures are an order of magnitude higher at the same densities, making allowed GT transitions the dominant contributor to electron capture rates.

In the astrophysical environment, the weak interaction processes have been modified due to screening effects. The screening corrections for electron capture have been developed in [13] and the extension to beta decays was given in [51]. There are two important effects induced by the astrophysical environment. First, screening enlarges the energy threshold for electron capture. Second, it reduces the electron's chemical potential. Both effects together reduce the electron capture rates, while they enhance beta decay rates. Rate modifications due to screening are relatively mild, on the order of a factor of two. The effects for the URCA pair ^{25}Na–^{25}Mg are shown

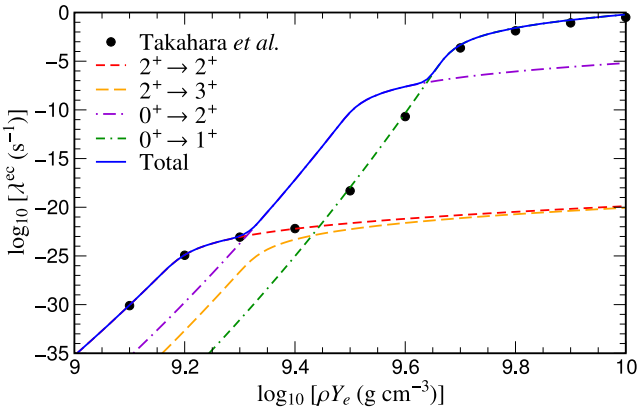

Figure 14. Electron capture rate for ^{20}Ne as function of density and for a specific temperature. The rate labeled 'Takahara *et al*' was evaluated using GT distributions calculated within the shell model [47]. The rate is broken down into the individual state-by-state contributions, where the energies and transition strengths are all taken from experiment. The label '$0^+ \rightarrow 2^+$' identifies the contribution from the second forbidden ground-state-to-ground-state transition, whose strength has been measured by Kirsebom *et al* [52]. This transition dominates the capture rate at the densities most relevant for the core evolution of intermediate-mass stars. Reprinted figure with permission from [51], Copyright (2014) by the American Physical Society.

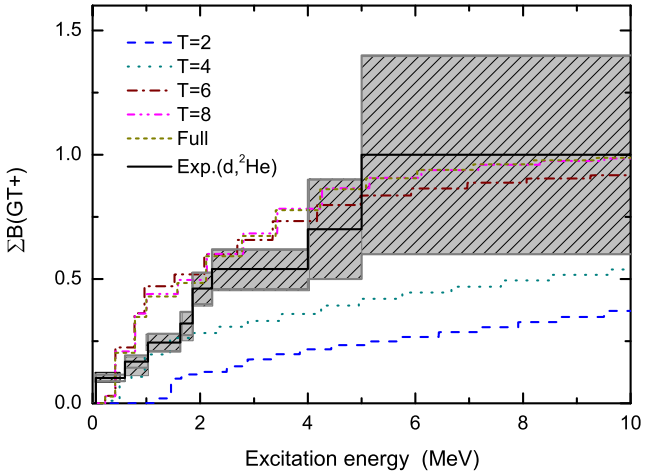

Figure 15. Comparison of experimental GT strength distribution for ^{76}Se (shown as a running sum) with the results obtained by shell-model diagonalization using the RG residual interaction and different levels of truncation. Reprinted from [147], Copyright (2011), with permission from Elsevier.

in figure 13. Modifications of the electron capture rates due to screening during the collapse of a massive star are discussed in [13] and exemplified in their figure 10.

3.2. Electron capture on nuclei with $A > 65$

Shell-model studies of nuclei with mass numbers $A \geqslant 65$ require an accurate description of cross-shell correlations. The associated model spaces generally make diagonalization shell-model calculations infeasible. It is fortunate that by the time nuclei with $A \geqslant 65$ dominate the core composition, the density, and accordingly the electron's chemical potential, have grown sufficiently that the capture rates are mainly sensitive to the total GT strength and its centroid. For these nuclei, an HM [36, 39] has been proposed to evaluate the stellar capture rates. In this model, the rates are calculated using an RPA approach in appropriately large model spaces using partial occupation numbers. These occupation numbers are calculated using the SMMC method [40, 41] and hence consider the relevant multi-particle–multi-hole configurations required to properly describe the cross-shell correlations which are relevant for nuclei in this mass range. Moreover, the SMMC determines the nuclear properties at a finite temperature, as is appropriate for the astrophysical environment. The RPA approach is known to reproduce the strength and centroids of collective excitations. However, it does not usually give a full account of the fragmentation of the strength which, as explained above, might not be needed under the astrophysical conditions at which the heavy nuclei studied by the HM appear during the collapse. Typically, the Fermi energy of the electron gas is noticeably larger than the Q value of the respective nuclei, requiring only the reproduction of the total strength and its centroid for a reasonable estimate of the rate.

The SMMC calculations of the partial occupation numbers have been performed in large model spaces (pf–sdg for nuclei with neutron numbers $N \leqslant 61$ and $pf_{5/2}$–sdg–$h_{11/2}$ for even heavier nuclei) using an adjusted pairing and quadrupole interaction to avoid the infamous sign problem [41]. The HM has been validated in [13] and applied to about 250 nuclei in the mass range $A = 66$–120 [13, 39].

In this context, ^{76}Se with $Z = 34$ and $N = 42$ is a special nucleus, since its GT$_+$ strength vanishes in the IPM (and in the Bruenn parametrization used in supernova simulations prior to 2003 [18]). The GT strength has been experimentally determined using the (d,^{2}He) charge-exchange technique at Groningen [38] proving that cross-shell correlations indeed unblock the GT strength (see figure 15). Diagonalization shell-model calculations, performed in different model spaces and with different residual interactions, are able to describe the low-energy spectra of ^{76}Ge and ^{76}Se and also the GT strength (figure 15). These shell-model calculations showed that cross-shell correlations are a relatively slowly converging process requiring the inclusion of multi-particle–multi-hole configurations. For example, the consideration of 2p–2h configurations alone does not suffice to move enough GT strength to low energies (figure 15).

We note that ^{76}Se, being an odd–odd nucleus, is never very abundant during core collapse. Nevertheless, figure 16 compares the electron capture rates calculated from the experimental and diagonalization shell model (for different interactions and model spaces) GT distributions with those obtained from the HM for two different core densities and for various temperatures [147]. The lower density corresponds to presupernova conditions, where electron capture is dominated by pf shell nuclei. The rates calculated from the data and the shell-model GT strength distributions agree quite well. The HM rates agree with the other rates to within a factor of three for the range of temperatures given, but they show a distinctly different T-dependence. This is related to the fact that the HM does not

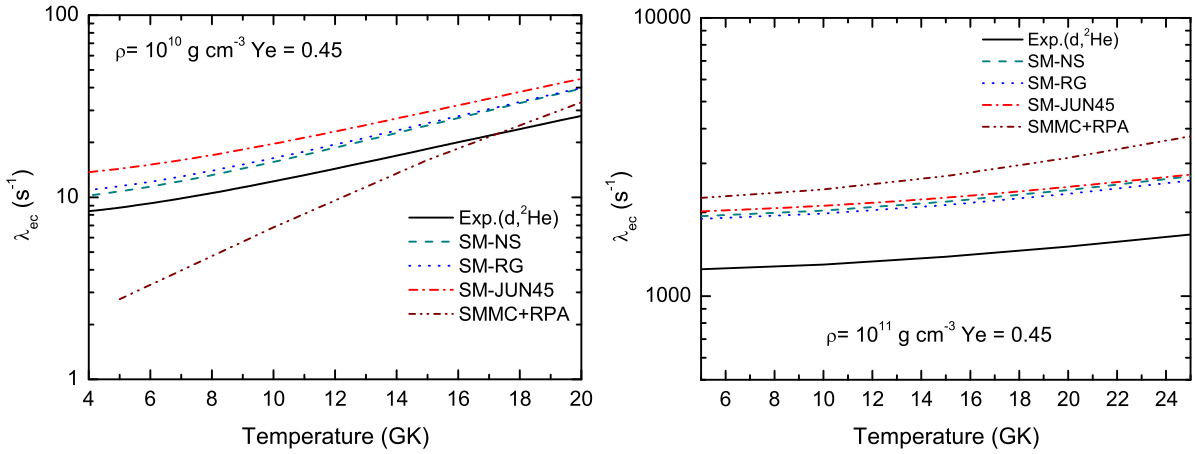

Figure 16. Electron capture rates on ^{76}Se at $\rho = 10^{10}$ g cm^{-3} (left) and $\rho = 10^{11}$ g cm^{-3} (right) as a function of temperature. The rates have been calculated from the experimental ground-state data [38] and by diagonalization shell model approaches that use different residual interactions. The results labeled 'SMMC + RPA' have been obtained within the HM. Reprinted from [147], Copyright (2011), with permission from Elsevier.

resolve the fragmentation of the GT strength, which is particularly important at low temperatures and densities. In fact, at the higher density, the agreement between all rates is quite satisfactory. Under these conditions, the electron chemical potential is noticeably larger than the capture Q-value, making the rate less sensitive to the details of the GT distribution. The HM calculation also considers forbidden multipoles, whose contributions increase with temperature but are relatively small [147]. We note that the shell model and experimental rates are solely determined from the ground-state GT distribution, while the HM considers finite temperature effects in the calculation of the occupation numbers. These turn out to be less relevant, as the $N = 40$ gap is already strongly overcome by correlations in the ground state. This will be different for the $N = 50$ gap, discussed below.

The thermal quasiparticle RPA (TQRPA) model [148] is an alternative approach proposed for the calculation of electron capture (and neutrino-nucleus reaction) rates at finite temperatures [44, 149]. Like the SMMC, the TQRPA is also based on an equilibrium statistical formalism and treats the many-nucleon system in a heat bath and a particle reservoir in the grand canonical ensemble. The method can be understood as a proton–neutron QRPA approach extended to finite temperatures that allows the determination of temperature-dependent spectral functions which are the basis for evaluating weak-interaction rates within this model [44]. Further extensions allow the use of Skyrme [149, 150] and relativistic functionals [151] to describe the thermal state and its excitation by considering 2p–2h correlations.

Compared to the HM, the TQRPA has the advantage of being formally consistent in treating the many-body problem. In contrast, the two parts of the HM have different complexities in dealing with the many-body states. It turns out, however, to be important that the SMMC considers multi-particle–multi-hole correlations, as will be discussed below.

The TQRPA approach has been used to calculate electron capture at finite temperatures for selected Fe and Ge isotopes [44] and for nuclei at the $N = 50$ shell closure [45, 149]. The differences between the two models are illustrated in figure 17, which compares the electron capture rates calculated in both approaches for various neutron-rich Ge isotopes at different densities and temperatures. In general, as the electron chemical potential grows with density and temperature, the rates increase as well, with more sensitivity to density than to temperature. The rates decrease with increasing neutron numbers. There are two reasons for this. Foremost, the Q value increases, but the occupation of the $g_{9/2}$ neutron orbital also grows, decreasing the unblocking of pf-shell neutron orbitals. Neutron-rich Ge isotopes appear in the core composition at temperatures $\gtrsim$1 MeV and densities $\rho Y_e, \gtrsim, 10^{11}$ g cm^{-3} and both models predict quite sizable capture rates for these conditions. There are, however, differences between the two models. In general, the HM capture rates are larger than those obtained in the TQRPA, most evidently at lower densities. Furthermore, the TQRPA model shows a steeper increase of the capture rates with temperature than the HM. These facts are primarily related to the increased unblocking probabilities in the HM due to many-body correlations which result in larger GT strengths at lower excitation energies. The differences in the rates become smaller with increasing density and temperature. This is mainly due to the growing electron chemical potential, which makes the rate less sensitive to the details of the GT strength distribution. Secondly, forbidden transitions increasingly contribute with growing density and temperature. These contributions are not subject to blocking effects.

We have seen that many-body correlations already overcome the $N = 40$ shell closure in the ground state and unblock the GT contribution to the capture rate. But what happens at the magic number $N = 50$? In fact, measurements of the GT$_+$ distribution for ^{86}Kr ($Z = 36$ and $N = 50$) [106] and for ^{88}Sr ($Z = 38, N = 50$) show only very little strength, mainly located at excitation energies between 8–10 MeV [107]. This points to a rather strong blocking of GT transitions at $N = 50$. The electron capture rates calculated from the experimental ground state data are indeed significantly lower than expected from systematics [107]. The results for ^{86}Kr and ^{88}Sr

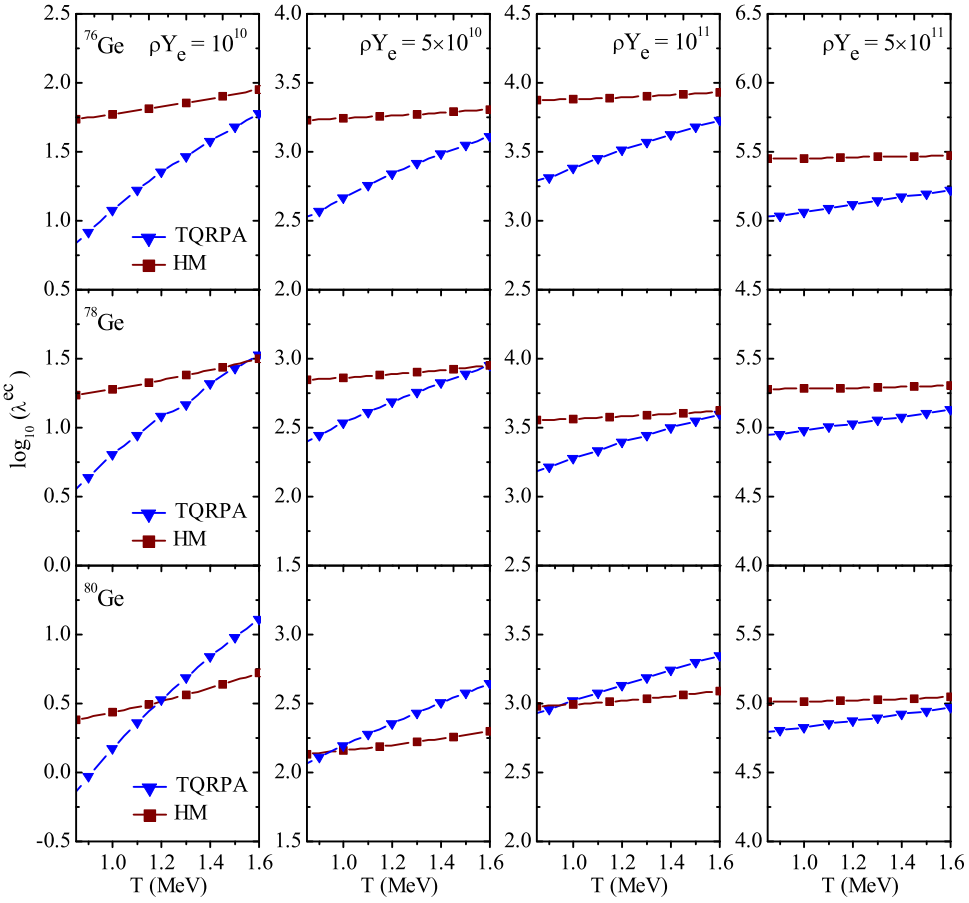

Figure 17. Comparison of electron capture rates for ^{76,78,80}Ge for different densities ρY_e and as a function of temperature, calculated using the TQRPA and HM. Reprinted figure with permission from [44], Copyright (2010) by the American Physical Society.

are surprising, given that a significant amount of GT strength ($\sim$0.7 units) was observed for ^{90}Zr [152] even though, based on transfer reaction experiments [153], the proton $0g_{9/2}$ occupation numbers for ^{88}Sr and ^{90}Zr are comparable: 0.7 and 1.0, respectively. A high-resolution experiment for ^{90}Zr is necessary to better understand these results.

In the collapsing core, $N = 50$ nuclei (e.g. ^{82}Ge and ^{78}Ni with Y_e values of 0.39 and 0.34, respectively) are very abundant at densities in excess of about 10^{11} g cm^{-3} [4, 154] and at temperatures $T > 1$ MeV. At these high temperatures, the average nuclear excitation energy is about $\langle E \rangle = 10$ MeV, which is larger than the $Z = 28$ proton gap and the $N = 50$ neutron gap. This implies that capture at stellar temperatures occurs, on average, in states with important many-body correlations across the two gaps, in this way unblocking the GT contribution to the capture rate. This is indeed born out in TQRPA calculations performed for $N = 50$ nuclei between ^{78}Ni and ^{88}Sr. The capture rates obtained are shown in figure 18. Satisfyingly, the TQRPA calculations find no GT strength in the ^{86}Kr and ^{88}Sr ground states at low energies, which is in agreement with observations. In fact, the TQRPA capture rates, calculated solely from the $T = 0$ GT distributions, agree with those obtained from the experimental GT distributions for both nuclei (see figure 18). However, the TQRPA calculation shows a strong thermal unblocking of the GT strength as protons are moved into the $g_{9/2}$ orbital and neutrons out of the pf shell. This leads to a strong increase in the capture rate for all nuclei (see figure 18). Thermal unblocking of the GT strength has the largest effect at small electron chemical potentials μ_e (low densities), while its relative importance decreases with growing μ_e. With increasing density, contributions from forbidden transitions become more important and dominate the rate for densities on the order of ρY_e, $\gtrsim$, 10^{11} g cm^{-3}, hence, at the conditions where $N = 50$ nuclei are abundant in the collapse. The capture rates also increase with increasing proton numbers, i.e. from ^{78}Ni to ^{88}Sr. This has two reasons: the growing Q value with neutron excess, and the increased promotion of protons into the $g_{9/2}$ orbital.

In summary, GT measurements for nuclei that become relevant in the high density/temperature environment during supernova collapse are indispensable to constrain nuclear models and to create trust in them. However, they cannot be used to directly determine the stellar capture rate, since thermal unblocking effects noticeably modify the rates under such conditions. This is particularly true at shell closures, i.e. for $N = 50$ nuclei. For these nuclei, forbidden transitions might be as relevant as GT transitions and should be experimentally constrained as well.

Figure 18 also shows the rate estimated by a parametrization proposed in reference [39]. This simple parametrization

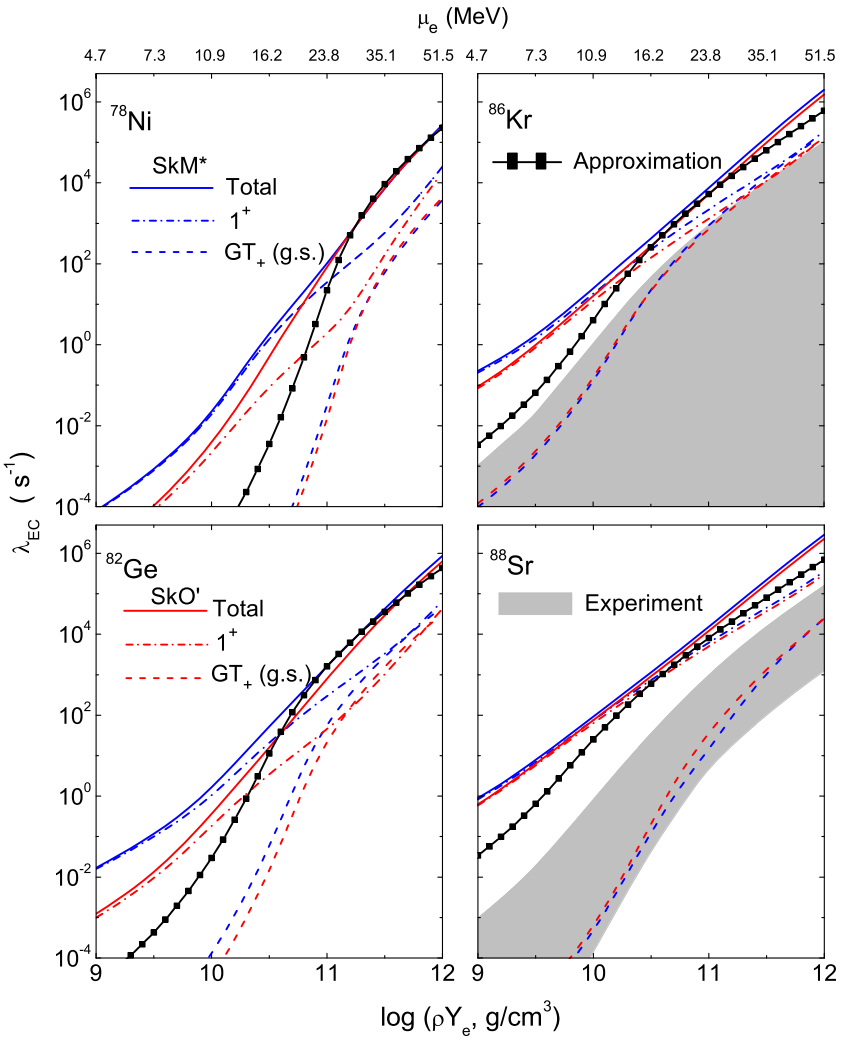

Figure 18. TQRPA electron capture rates for selected $N = 50$ nuclei calculated at $T = 0$ and at $T = 1$ MeV and as a function of density. The upper axis shows the corresponding electron chemical potential. The calculations were performed for two Skyrme interactions: SkM* (blue lines) and SkO' (red lines). The calculated total capture rates also include contributions from forbidden transitions; the GT contribution is presented individually. The shaded area is the rate obtained from the experimental ground-state GT distribution (taken from [107]). The thick line labeled 'approximation' represents the 'single state approximation' adopted from [39]. Reprinted figure with permission from [45], Copyright (2020) by the American Physical Society.

assumes that the capture proceeds through a single transition from an excited state in the parent nucleus at E_i to a state in the daughter nucleus at E_f with $\Delta E = E_\mathrm{f} - E_\mathrm{i}$ (a single-state approximation). The capture rate can then be written as [16]

$$\lambda = \frac{\ln(2)B}{K}\left(\frac{T}{m_\mathrm{e}c^2}\right)^5 \left[F_4(\eta) + 2\chi F_3(\eta) + \chi^2 F_2(\eta)\right], \quad (4)$$

where $\chi = (Q + \Delta E)/T$, $\eta = (\mu_\mathrm{e} - Q - \Delta E)/T$, $K = 6146$ s, and B represents a typical (GT plus forbidden) matrix element. The quantities F_k are the relativistic Fermi integrals of order k. Q is the ground-state-to-ground-state Q-value that is positive for capture in protons and neutron-rich nuclei. This approximation was used in references [39, 42] to estimate the rates of the many heavy nuclei which are abundant at larger densities and for which no rates existed at that time. The two parameters (energy position and GT strength) were fitted to the rates of about 200 nuclei for which individual *pf* shell-model and HM rates were available. Figure 19 compares the shell-model rates with the single-state approximation (4) using $B = 4.6$ and $\Delta E = 2.5$ MeV. We note that the approximation does not consider nuclear structure effects (or a dependence on the average excitation energy), which result in a quite significant scatter of the shell-model rates with respect to the single-state rate. For the reasons discussed above, the fluctuations are noticeably reduced with increasing density. It is worth noting that there is no systematic difference between the approximation and the shell-model rates, so differences might at least partially cancel out. At intermediate densities, the single-state approximation shows some tendency to overestimate the rate. In conclusion, the approximation in its simple form (4) should not be used at low densities, below a few 10^{10} g cm^{-3}. In this density regime, the nuclear composition is largely dominated by nuclei for which shell-model rates exist. The general trend seen in figure 19 is also borne out in figure 18,

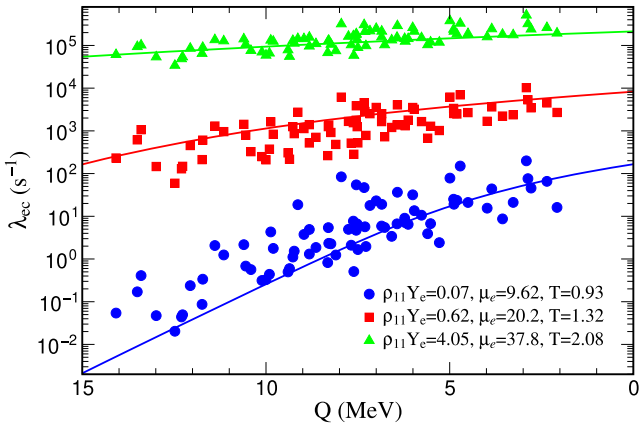

Figure 19. Electron capture rates on nuclei, for which individual shell model rates exist, as a function of the Q value for three different stellar conditions. Temperatures are measured in MeV, density in 10^{11} g cm^{-3}. The solid lines represent the rates obtained from the single-state approximation (4). Reprinted figure with permission from [39], Copyright (2003) by the American Physical Society.

where the approximation fails badly at low densities, but gives reasonable agreement at $\rho Y_e \gtrsim 10^{11}$ g cm^{-3}. Reference [154] compares the shell-model and single-state rates under slightly different astrophysical conditions.

The single-state parametrization has been adopted for heavy nuclei in supernova simulations which systematically studied the influence of nuclear ingredients (electron capture rates, equation of state, mass models) on the collapse dynamics [154, 155], while reference [155] used the improved single-state parametrization of [156] (see section 4.1).

3.3. Rate tables

Most supernova codes now use the rate table provided by Juodagalvis *et al* [13]. This table defines electron capture rates on a grid of the three important parameters characterizing the astrophysical conditions during collapse: temperature, density, and Y_e value. The rate evaluation assumes that the core composition is given by NSE, hence it does not provide rates for individual nuclei.

The rate table is based on the hierarchical strategy defined above. For nuclei with $A < 65$, the shell model rates of Oda *et al* [33] (*sd* shell) and of Langanke and Martínez-Pinedo [34] (*pf* shell) have been adopted. This guarantees a reliable and detailed reproduction of the GT strengths for the important nuclei at collapse conditions where $\mu_e \sim Q$. The rates for nuclei in the range $A = 39$–44 have been taken from Fuller, Fowler, and Newman [3]. For the heavier nuclei, the table adopts the rates given by HM calculations. For about 200 nuclei in the mass range $A = 65$–110, these were calculated by using SMMC partial occupation numbers in RPA calculations. For a few nuclei in this mass regime and for even heavier nuclei, a total of about 2700 nuclei, the rates were evaluated on the basis of a parametrization of the occupation numbers (derived in accordance with the SMMC studies) and RPA response calculations. In this way, the most relevant nuclear structure inputs, such as shell gaps, are accounted for. Screening corrections due to the astrophysical environment have been incorporated into the rates.

We note that for astrophysical conditions with temperatures below $\sim$4 GK, NSE is not achieved, and detailed bookeeping of the individual reactions is necessary to determine the composition. This occurs during silicon burning, for which the *sd* and *pf* shell nuclei are relevant. Hence the knowledge of individual rates is essential.

Weak-interaction rates for *sd* shell nuclei are important for the core evolution of intermediate-mass stars. Rates for individual nuclei for the relevant density and temperature regime are given in [33] and updated in [50].

Nuclei in the mass range $A = 45$–65 are essential for the early phase of core collapse supernovae and for nucleosynthesis in thermonuclear (type Ia) supernovae. The weak-interaction rates for these *pf* shell nuclei are individually given in [34]. At present, weak-interaction rates based on the diagonalization shell model do not exist for nuclei in the mass range $A = 39$–44. Studies of these nuclei require the inclusion of correlations across the $Z, N = 20$ shell closures and hence large model spaces enabling allowed GT and also forbidden transitions. Steps have been taken to performing these demanding calculations, so a shell-model evaluation also appears to be in reach for this mass range. Weak-interaction rates for $A = 39$–44 were provided by Fuller *et al* in their seminal work based on the IPM, but also by Nabi and Klapdor-Kleingrothaus within the framework of the QRPA [157]. The latter reference gives electron capture rates for a wider range of nuclei. Many tabulations of electron capture rates (e.g. references [3, 14–16, 33, 34, 157, 158] do not include screening corrections. Reference [13] presents a formalism that describes how these rates can be approximately corrected for screening effects.

To make it easier to incorporate complete sets of electron-capture rates in astrophysical simulations, a library of rates was created [154, 159, 160] based on the rate tables for specific mass regions described above and on the single-state approximation for nuclei where rates based on microscopic calculations are not available. This library has been incorporated into the weak-rate library NuLib [161].

3.4. Next steps in evaluating stellar electron capture rates

What progress can we expect in the theoretical modeling of stellar electron capture in the midterm future, particularly as we are on the eve of computational breakthroughs such as exascale computing? Such progress, accompanied by appropriate advances in computer memory, will certainly pay off in terms of the nuclei for which diagonalization shell-model calculations will become possible. First, this will allow us to perform calculations for the nuclei around mass number $A = 40$, which requires the inclusion of levels from the *sd* and *pf* shells, completing the shell-model evaluation of capture rates of nuclei with mass numbers $A < 65$, which dominate the capture process during the early supernova collapse phase. Second, shell-model calculations in the complete *pf*-$g_{9/2}$ shell will become possible, which will be exploited to systematically study the unblocking of the GT strength at the

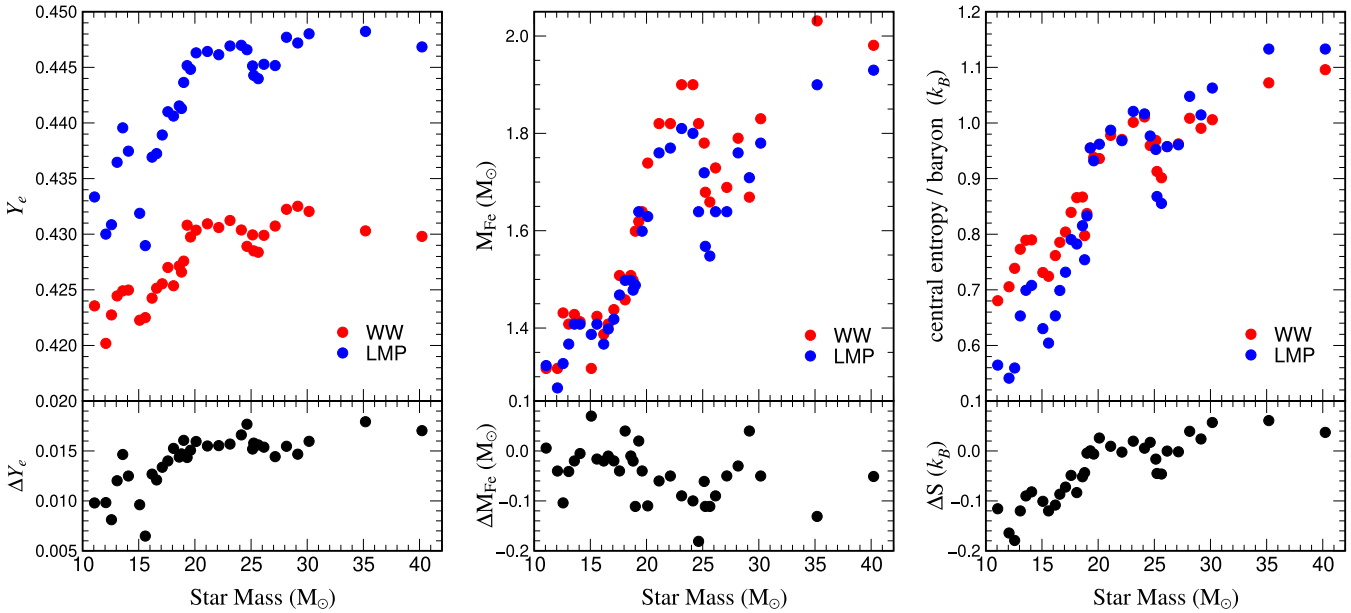

Figure 20. Comparison of the center values of Y_e (left), the iron core sizes (middle) and the central entropy (right) for $11-40M_\odot$ stars between models using the FFN rates (WW models [167]) and models which used the shell-model weak interaction rates (LMP [35]). The lower panels show the changes in the three quantities between the WW and LMP models. Reprinted figure with permission from [28], Copyright (2003) by the American Physical Society.

$N = 40$ shell gap. As discussed above, the pioneering shell model work performed for ^{76}Se mainly concentrated on the unblocking of the strength by correlations in the ground state. However, the respective mid-mass nuclei play a role during the collapse at finite temperatures. Thus, supplementing the shell-model studies which explore how thermal excitations support the unblocking mechanism is quite desirable, as such effects are difficult to study experimentally. However, direct state-by-state evaluation of the capture rates at the respective temperatures is impractical, due to the plethora of parent states on which the captures can occur. Here, one clearly has to rely on statistical approaches. Nevertheless, progress is conceivable in various ways. This is particularly important to decisively determine how strongly nuclei at the $N = 50$ shell closure act as obstacles to capture at the modest temperatures prevailing in the core when such nuclei become abundant. A consistent evaluation of such capture rates within the SMMC formalism might be desirable and conceivable if the two challenges currently hampering these studies can be overcome. These are the sign problem encountered when realistic residual interactions are used [41, 162] and the numerical challenges involved in performing the inverse Laplace transformation needed to calculate the GT (and other) strength functions [163, 164]. On the positive side, both problems become less relevant with increasing temperatures. Since SMMC studies scale nearly perfectly with the number of computer nodes [41], such calculations will obviously benefit from improved computer infrastructure.

As discussed above, an alternative statistical model based on the QRPA formalism at finite temperatures has been used to calculate stellar electron capture rates. These approaches have very recently been extended to incorporate additional correlations and have been applied to the calculation of stellar capture rates for selected nuclei [165, 166]. Further extensions of these methods to deformed and odd–A nuclei are very desirable.

4. Electron capture in astrophysical applications

4.1. Core-collapse supernovae

Simulations of the evolution of massive stars distinguish two distinct phases, motivated by their specific needs and requirements. (1) During hydrostatic burning, energy released by nuclear reactions in the star's interior is essential to balance gravity. The densities are low enough that neutrinos, produced in weak interactions, can leave the star unhindered, transporting energy away. This loss has to be considered in the energy balance, but a detailed treatment of neutrino transport is not required. However, the simulations have to incorporate a detailed network of nuclear reactions to follow the nuclear energy production and the change in composition. This stellar evolution period lasts to the so-called presupernova phase, when the core density has reached values of about 10^{10} g cm^{-3} and the inner part of the iron core collapses with velocities in excess of 1000 km s^{-1} [29, 167].

The final models obtained by the stellar evolution codes become the input for the supernova codes in which the gravitational collapse of the iron core and the explosion are simulated. The astrophysical conditions relevant during these simulations lead to two important changes compared to stellar evolution. The temperatures are sufficiently high in the core ($T, \gtrsim, 4$ GK) that the nuclear composition can be accurately approximated by an NSE distribution, without the need to follow a complicated network of nuclear reactions. On the other hand, the densities involved require detailed neutrino

bookkeeping. This is achieved by neutrino radiation transport. An additional complication arises from the fact that the assumption of spherical symmetry is not valid during the core collapse and explosion. This requires multidimensional treatments, which are extremely challenging and computationally demanding. Reviews of the recent impressive progress in supernova modeling can be found in [168–172]. These codes, in general, consider electron capture via the rates provided by [13].

Heger *et al* investigated the effect of diagonalization shell-model rates on the presupernova evolution of stars in the mass range $M = 13$–$40M_{\odot}$ [29, 35]. To this end they repeated the calculations of Weaver and Woosley [167], keeping the stellar physics as similar as possible, but replacing the weak interaction rates for the pf shell nuclei by those of reference [34] (LMP rates). Figure 20 summarizes the consequences of the shell-model rates on three quantities which are relevant for the following collapse. The central $Y_{\rm e}$ value is larger by $\Delta Y_{\rm e} = 0.01$–0.015 at the onset of collapse. There are two reasons for this. First, the shell-model rates are noticeably smaller than the FFN rates (figure 12), and therefore reduce leptonization. Second, during silicon burning, β decay can compete with electron capture. Although this does not occur according to specific URCA pairs, but rather by an ensemble of nuclei, the effect is the same: the star is additionally cooled, while $Y_{\rm e}$ is kept constant. The study confirmed that β decay becomes increasingly Pauli blocked with growing density and can be safely neglected during collapse. Figure 20 also indicates that the iron core masses are generally smaller with the LMP rates. However, this is not a continuous effect and shows variation among models with different stellar masses. Finally, the LMP rates lead to presupernova models with lower core entropy for stars with $M < 20M_{\odot}$. For the more massive stars, the effect is not unique; stars with $M = 30$–$40M_{\odot}$ show an increased core entropy. We should mention that lower (larger) core entropy implies less (more) free protons in the nuclear composition, which, however, is overwhelmingly dominated by nuclei.

Continuous electron capture drives the NSE composition of the core to be more neutron-rich and toward heavier nuclei. At densities in excess of a few 10^{10} g cm^{-3}, the composition is dominated by nuclei with $Z < 40$ and $N > 40$, for which it was assumed for a long time that electron capture vanished (e.g. [18]) due to Pauli blocking of the GT strength. As a consequence, the capture process later in the collapse was thought to continue solely on free protons, which are, however, less abundant than heavy nuclei by orders of magnitude. As we have discussed in section 3.2, the GT strength at the $N = 40$ shell gap is unblocked by multi-nucleon correlations. Furthermore, the blocking at the $N = 50$ shell closure, which results in a strong reduction in the experimental ground-state GT strength, is overcome under finite-temperature core conditions by thermal excitation.

Arguably the most important result reported in references [39, 42] is the fact that electron capture proceeds on nuclei rather than on free protons during the entire collapse, in contrast to previous belief (e.g. [1]. These findings are based on supernova simulations performed independently by the Garching and Oak Ridge groups, which both adopted the HM capture rates for more than 100 nuclei in the mass range $A = 65$–110, supplemented by the shell-model rates for pf shell nuclei. For the heavy nuclei, the capture rates were estimated by the single-state approximation. The capture rate on free protons was taken from [18].

Figure 21 compares some important quantities obtained in the simulations of references [39, 42] with previous studies which neglected electron capture on heavy nuclei. Obviously, the capture on nuclei is an additional source of deleptonization, adding to the capture on free protons. This results in significantly lower values for $Y_{\rm e}$ on neutrino trapping at densities of around 10^{12} g cm^{-3}. At higher densities, the total lepton fraction $Y_{\rm lep}$ becomes constant, while the electron fraction $Y_{\rm e}$ still decreases. This is related to neutrino trapping and the formation of the homologous core [1]. In this regime, continuous electron capture reduces the electron abundance, but the neutrinos generated by this process mainly interact with matter by coherent scattering on nuclei at a rate sufficiently large that their diffusion timescale is longer than the core collapse timescale. Neutrinos are trapped, adding to the total lepton fraction in the core and leading to neutrino Pauli blocking of further electron capture. However, before trapping, the neutrinos can still leave the star and are an additional cooling mechanism leading to smaller core entropies than those obtained in previous calculations. Lower entropies reduce the abundance of free protons in the NSE composition, which increases the importance of capture on nuclei due to their increased abundance. Neutrinos produced by capture on nuclei have smaller average energies due to their higher Q-value compared to neutrinos produced by capture on free protons. Hence, the luminosity of electron neutrinos is increased due to more captures, but their average energies are shifted to lower values. We stress that the rate for capture on individual nuclei is noticeably smaller than the capture rate on free protons. The dominance of capture on nuclei is a result of the overwhelmingly higher abundance of nuclei compared to free protons and is a result of the low entropy, i.e. of the capture process.

The fact that electron capture on nuclei proceeds until neutrino trapping occurs is also reflected in the core dynamics and profiles. In the simulations with the improved rates, as shown in figure 22, the shock forms with significantly less included mass (a smaller 'homologous core' size) and a smaller velocity difference across the shock. Despite this mass reduction, the radius from which the shock is launched is actually pushed outwards slightly, due to changes in the density profile. Despite these significant alterations, one-dimensional supernova models employing the new electron capture rates still fail to explode. No noticeable differences in the simulations are observed if the rate set of Juodagalvis *et al* [13] is used, which replaces the rates for nuclei (for which, in [42], the single-state approximation was used) by rates estimated in the spirit of the HM. Multidimensional supernova simulations now describe electron capture using the rates of reference [13]. However, no dedicated investigation of the role of electron capture (i.e., in comparison to the case where capture on heavy nuclei is neglected) has been performed.

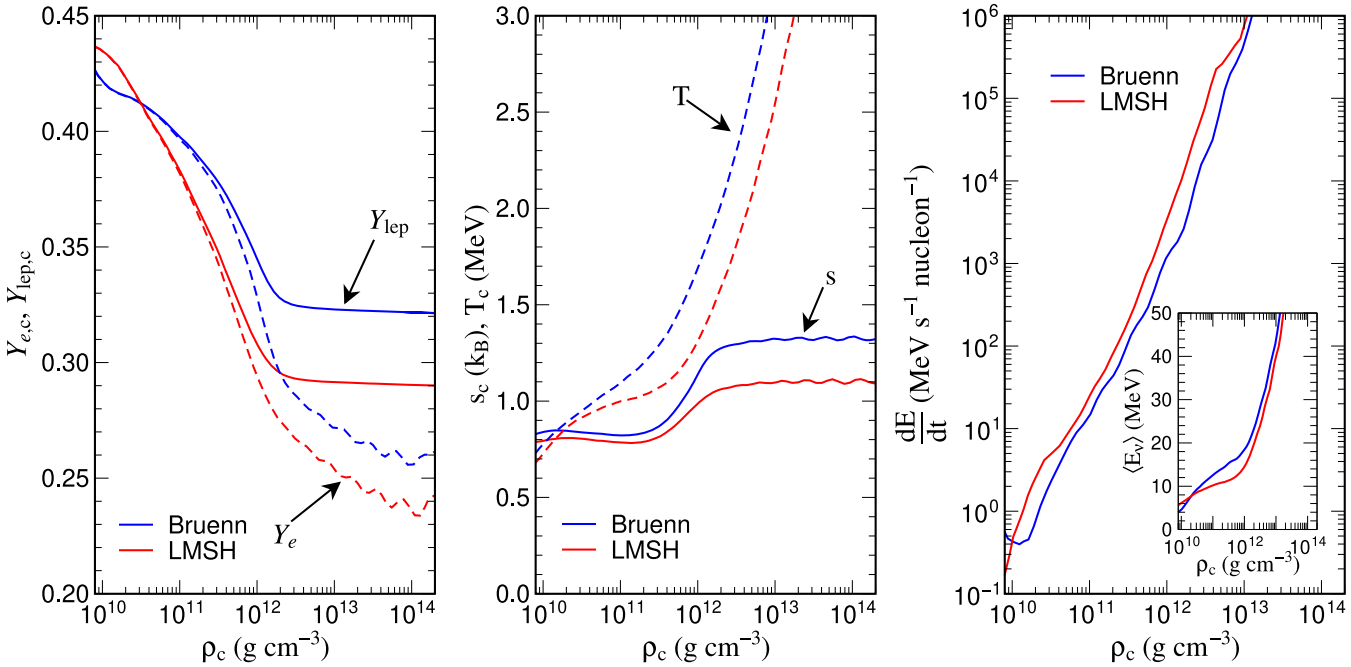

Figure 21. Comparison of a supernova simulation for a $15M_\odot$ star using the shell-model weak interaction rates from reference [28] (labeled LMSH) and the Bruenn parametrization, which neglects capture on nuclei for $N > 40$ [18] (labeled Bruenn). The figure shows the central core values for Y_e and Y_{lep} (electrons plus neutrinos) (left), the entropy and temperature (middle), and the neutrino emission rate (right) as a function of core density. The insert in the right-hand figure shows the average energy of the emitted neutrinos. Reprinted from [25], Copyright (2006), with permission from Elsevier.

In a recent supernova simulation [173], electron capture on nuclei has been identified as the dominant weak-interaction process and the main source of electron neutrinos during collapse. However, it was shown that pair-de-excitation of thermally excited nuclear states is an important source of the other neutrino types (electron anti-neutrinos, muon and tau neutrinos and their antiparticles).

The contribution of a particular nucleus to the reduction of Y_e during collapse depends on the product of its abundance and its capture rate. Both quantities are time-dependent and have to be integrated over the duration of the collapse. This study has been performed by Sullivan *et al* [154] using rates calculated based on microscopic nuclear models, where available. For the heavy nuclei, for which such rates are not individually available, they adopted the single-state approximation of equation (4).

The upper panel of figure 23 shows which nuclear ranges contribute to the change of Y_e over time, $\dot{Y}_e$. The top axis shows the time until bounce. The corresponding densities are 1.41×10^{11}, 4.06×10^{11}, and 1.42×10^{12} g cm^{-3} at $t - t_b = -20, -10$, and -5 ms, respectively. We note that $\dot{Y}_e$ grows with time during collapse and reaches its maximum after trapping has already started. The increase reflects the fact that the electron chemical potential grows faster than other scales, in particular, the average nuclear Q value of the composition, resulting in strong increases of the capture rates. The change in the capture rate is mainly driven by nuclei in the mass range $A = 65$–105. The rates calculated within the HM exist for about 200 nuclei in this mass range, which, however, does not cover all nuclei that contribute. The *pf* shell nuclei, for which accurate diagonalization shell-model rates exist, dominate in the early collapse. Here, capture rates are, however, smaller due to the smaller electron chemical potentials involved. Nuclei heavier than $A = 105$ contribute or dominate just before and during trapping.

The lower panel of figure 23 identifies the contribution of individual nuclei to $\dot{Y}_e$, as determined by integrating the respective contributions during collapse until trapping occurs. Due to this study, the relevant nuclei are those around the $N = 50$ shell closure, centered in this range from ^{78}Ni to ^{82}Ge.

Sullivan *et al* [154] also investigated the effect of a systematic modification of the electron capture rates on the supernova dynamics. When scaling the capture rates for all nuclei by factors between 0.1 and 10, they observed significant modifications. A systematic reduction of the rates throttles the effects that capture on nuclei has during collapse, as outlined above, driving the results back toward those where capture on nuclei were neglected. A systematic rate reduction by a factor of ten indeed increases the enclosed mass at bounce by about 16%, which is a similar effect to that reported in reference [42]. Sullivan *et al* [159] and Pascal *et al* [155] argued that the single-state approximation might overestimate the rates for nuclei close to the $N = 50$ shell gap. A similar conclusion was drawn from the measurements of GT distributions for the ground states of the $N = 50$ nuclei ^{86}Kr [106] and ^{88}Sr [107]. As discussed above, the single-state approximation does not, in fact, consider nuclear structure effects which should be quite relevant, in particular at shell closures. We note that structural effects are considered in the shell-model rates used in reference [13] to set up a rate table for electron capture under

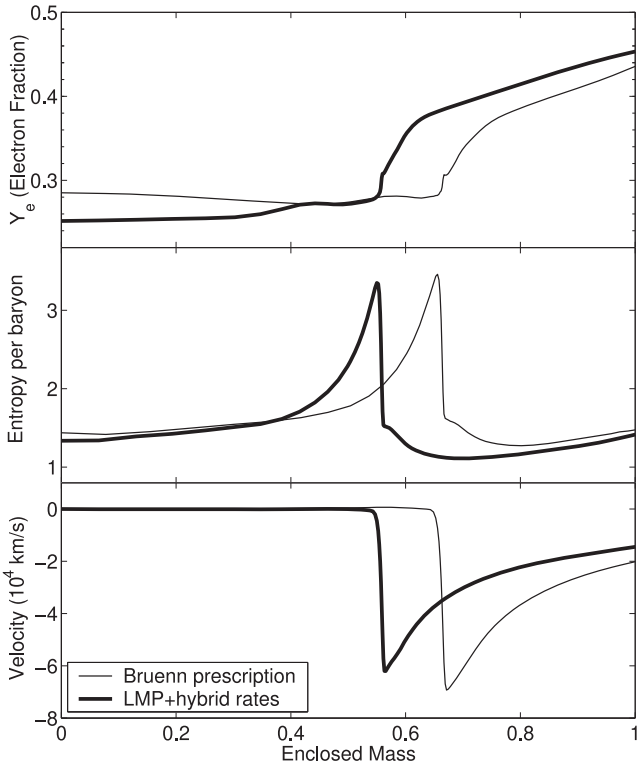

Figure 22. Comparison of Y_e (upper), entropy (middle), and velocity profiles (lower panel) at bounce obtained in supernova simulations using the shell-model rates for nuclei in the mass range $A = 45$–110 ([34, 39], thick line) and the Bruenn rate parametrization ([18], thin line). Reprinted figure with permission from [42], Copyright (2003) by the American Physical Society.

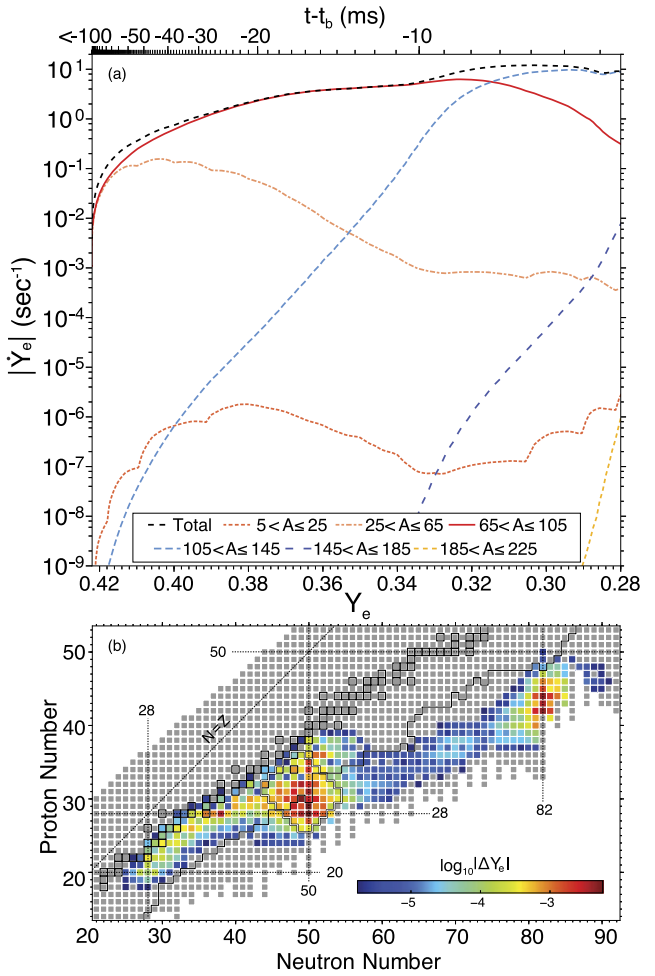

Figure 23. (Upper panel, a) The contribution of nuclear electron capture to the change of Y_e as function of Y_e which continuously reduces with time. As a reference, the upper axis indicates the time until bounce. (Lower panel, b) The top 500 nuclei that contribute most strongly to electron capture. Reproduced from [154]. © IOP Publishing Ltd. All rights reserved.

collapse conditions, assuming, however, NSE for the nuclear composition. It has been shown that the use of alternative and improved equations of state has rather small effects on supernova dynamics [154, 155]. The dependence of the core composition on different equations of state and its indirect impact on stellar electron capture rates has been investigated in references [174, 175]. An improved version of the single-state approximation is presented in [156]. The impact of a reduction of the $N = 50$ shell gap has been explored in reference [176]. We also mention again that the TQRPA calculations and the HM indicate that the blocking of the GT strength at around $N = 50$ is largely overcome under stellar conditions due to thermal unblocking. Furthermore, both models predict sizable contributions from forbidden transitions in the astrophysical conditions under which $N = 50$ nuclei are abundant during the collapse.

4.2. Nucleosynthesis in thermonuclear supernovae

Thermonuclear supernovae (observationally categorized as type Ia), form a class of supernova that is distinguished from the core-collapse version by its explosion mechanism and also by its spectral composition (type Ia spectra do not exhibit hydrogen lines, in contrast to the spectra of core-collapse or type II supernovae). In the currently favored model, type Ia supernovae correspond to the explosion of a white dwarf (WD) triggered by interaction with a binary companion. The companion can be either a main sequence, giant or helium star (single degenerate scenario) or another WD (double degenerate scenario) (for reviews see [177, 178]). WDs are compact objects produced as the final fate of intermediate-mass stars and stabilized by their electron degeneracy pressure up to a maximum mass on the order of $1.4 M_\odot$ (Chandrasekhar mass $M_{\rm Ch}$). WDs are mainly composed of $N = Z$ nuclei, i.e. ^{12}C, ^{16}O, ^{20}Ne.

The masses of WDs that explode in a type Ia supernova is another uncertain parameter. One distinguishes explosions of WDs with masses noticeably smaller than the Chandrasekhar mass (sub-$M_{\rm Ch}$ models) and with masses on the order of the Chandrasekhar mass (near-$M_{\rm Ch}$ models). In the latter case, high densities (10^8 g cm^{-3} and higher) are reached during the explosion. Under these conditions, the electron Fermi energies are high enough to induce electron capture on nuclei, which turns out to be important for the associated nucleosynthesis. The nucleosynthesis in various type Ia supernova scenarios has been studied in reference [179].

As an example of the impact of electron capture and its progressively advancing description, we refer to the studies performed for the W7 model [180], which has been regularly adopted in simulations of galactic chemical evolution. In this scenario, a WD with mass near $M_{\rm Ch}$ is assumed to be in a binary system with a companion star which enters the red-giant phase. The accretion from the companion adds to the WD's mass, bringing it toward the Chandrasekhar limit and increasing the density in its interior to the point where carbon burning can be ignited. As the burning occurs in a highly degenerate environment, the energy released cannot lead to expansion, but rather heats the surroundings. This results in a self-reinforcing acceleration of the burning until the degeneracy can be lifted and the entire WD is disrupted. The explosion mechanism—disruption of a WD in a thermonuclear runaway—leads to similarity among type Ia events. For example, the observed peak magnitude and the widths of the light curves obey a simple scaling law (Philipps relation [181]) which makes type Ia supernovae standard candles for cosmological distances. This fact has been exploited to deduce the current acceleration of our Universe.

After the burning flame has moved through the matter, the inner material behind the front, with a mass of about $1M_{\odot}$, reaches temperatures that are sufficiently high to drive the nuclear composition into NSE. As the WD was composed of $N = Z$ nuclei, ^{56}Ni is the main product. Deviations toward nuclei with excess neutrons occur due to electron capture in the hot and dense matter behind the front. The impact of this capture depends (besides the astrophysical conditions of density (about 10^9 g cm^{-3} and temperature ($T \sim 10^9$ K)) on the speed of the flame (i.e., the time available for electron capture before the star is disrupted) and obviously on the rates themselves. As discussed above, the diagonalization shell-model (LMP) rates are systematically lower than the FFN rates for *pf* shell nuclei, particularly for nuclei in the Ni–Fe mass range, which are of importance for captures behind the type Ia burning front. Brachwitz *et al* have performed nucleosynthesis studies in a one-dimensional supernova simulation based on the well-known W15 progenitor model of reference [180] which starts from a $1.38M_{\odot}$ C–O WD [10, 183]. The faster FFN rates lead to stronger deleptonization in the innermost $0.1M_{\odot}$ core mass, reaching values as low as $Y_{\rm e} = 0.44$ in the center, while the slower LMP rates produce $Y_{\rm e} = 0.45$ as the minimum value. As a consequence, the FFN rates predict an appreciable number of neutron-rich nuclei such as ^{50}Ti or ^{52}Cr, which are strongly overproduced compared to the solar abundances (left panel of figure 24). This overproduction constituted a serious problem [9], as roughly half of the ^{56}Fe contents of the solar abundances are synthesized in type Ia supernovae, and hence, for all nuclides produced in type Ia, overproduction factors larger than two place their relative abundances in conflict with observations. As is shown in the middle panel of figure 24, the overproduction is removed when the slower LMP shell-model rates are used. Suzuki has recently confirmed this finding in a study which replaced the LMP shell-model rates for selected nuclei in the Ni–Fe mass range with those obtained via the GXPF1 residual interaction, which gives better agreement with the measured GT strength in Ni isotopes [184]. Suzuki used a different progenitor model than reference [183] (the W7 model of [180]), but his study also shows that the overproduction of neutron-rich nuclei is removed if modern diagonalization shell-model capture rates are used, rather than the FFN rates (right panel in figure 24). Satisfyingly, Suzuki only observed a small difference of 4% in the calculated abundances based on his shell-model rates and on the LMP rates.

The studies of [9, 10, 183, 184] are based on spherically symmetric simulations. More recent three-dimensional studies of type Ia supernovae showed, however, the similar importance of electron capture in the high-density regime of the explosion that drives the nuclear abundance distribution to more neutron-rich nuclei. Detailed studies of the sensitivity of nucleosynthesis for various scenarios of type Ia supernovae can be found in references [48, 49, 179]. These simulations show that an NSE abundance distribution is reached in the high-density regime that produces nuclei in the iron–nickel mass range. One particularly interesting nucleus is ^{55}Mn, the only stable manganese isotope, which is produced in core-collapse and thermonuclear supernovae. Seitenzahl and collaborators made the important observation that ^{55}Mn must be overproduced relative to iron in type Ia supernovae to explain the solar [Mn/Fe] ratio, as all modern core-collapse simulations predict a [Mn/Fe] ratio noticeably smaller than the solar one [185]. As the high-density regime needed to produce manganese in thermonuclear supernovae is only achieved in near $M_{\rm Ch}$ scenarios, ^{55}Mn nucleosynthesis and its evolution over time in our Galaxy also places valuable constraints on the WD mass in the type Ia scenarios [179, 185, 186].

Electron capture and beta-decay, operating via URCA pairs (see section 3.1.2), are also important during the accretion and simmering phases of the evolution of CO WDs before the type Ia supernova explosion, as they determine the neutron excess and the density at which thermal runaway occurs [187]. Particularly important during these phases is the ^{13}N$(e^-, \nu_{\rm e})^{13}$C rate, whose value is determined using beta-decay and charge-exchange data [188].

4.3. Accreting neutron stars and mergers

An old isolated neutron star can be described as being in beta equilibrium. However, such an equilibrium is broken in the crust if the star accretes mass from the interstellar medium (ISM) or from a binary star. For an old neutron star traversing the ISM, a mass on the order of $10^{-16}M_{\odot}$ per year will be accreted as a layer on the neutron star's surface. The temperature of this layer is low and is usually approximated as $T = 0$ [189]. In a binary system, the mass flow can be higher, leading to the repeated burning of a surface layer accompanied by a characteristic emission of x-rays with typical durations of up to $\sim$100 s (x-ray burster [190, 191]). Due to the reoccurrence of the bursts, with typical periods on the order of a year, the ashes of previous events are pushed to higher densities and temperatures on the order of a few 10^8 K can be reached. These binary systems can also exhibit rare day-long x-ray bursts (so-called superbursts). Here, carbon flashes, triggered by the fusion of two ^{12}C nuclei, heat the

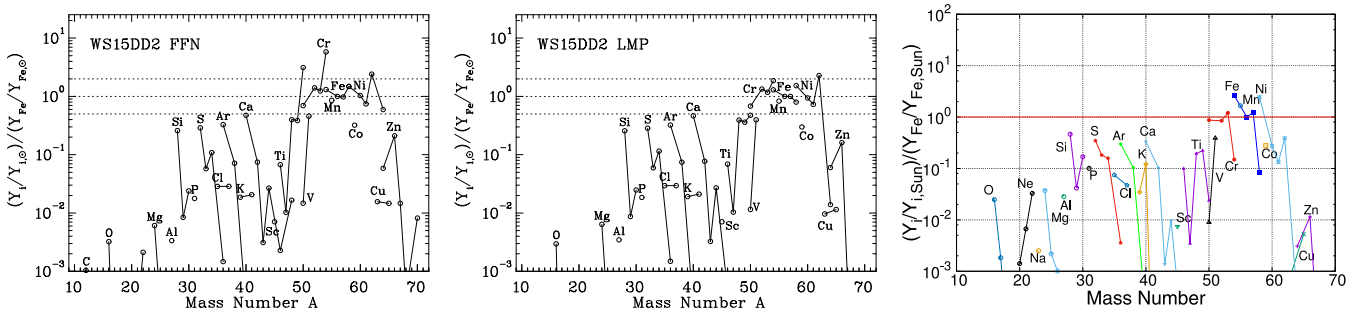

Figure 24. Influence of electron capture rates on type Ia nucleosynthesis. The two left panels show yields calculated for the WS15 progenitor model of reference [180] calculated with the FFN (left) and LMP (middle) electron capture rates (courtesy of F Brachwitz). (Left) Reprinted figure with permission from [28], Copyright (2003) by the American Physical Society. The right panel shows the yields calculated for the W7 progenitor model of reference [180] replacing the LMP rates with improved shell-model rates for selected nuclei in the Ni–Fe region. (Right) Reproduced from [182]. © IOP Publishing Ltd. All rights reserved. All yields are relative to the solar abundances. The ordinate is normalized to ^{56}Fe.

neutron star's envelope so that hydrogen and helium burning becomes stable, suppressing the usual shorter x-ray bursts. These can only occur after the envelope has cooled sufficiently [192]. Electron capture plays an interesting role in both accretion scenarios.

The ISM matter that an old isolated neutron star accretes is mainly hydrogen. At sufficiently high densities, hydrogen can start a sequence of nuclear reactions. However, in contrast to stellar hydrostatic burning, this is not initiated by temperature, but by density fluctuations triggering so-called pycnonuclear reactions [193, 194]. The nuclear reaction sequence includes hydrogen and helium burning, producing nuclides up to ^{28}Si. It is particularly challenging to evaluate the pycnonuclear triple-alpha reaction rate, as neither the ^{8}Be intermediate state nor the Hoyle state in ^{12}C can be thermally reached [195–197]. The fresh material produced by pycnonuclear reactions rests on original neutron-star crustal material, i.e. ^{56}Fe or ^{62}Ni.

Electron capture can occur once the density reaches a value at which the electron chemical potential can overcome the nuclear Q value. For ^{16}O, which is the main product produced by pycnonuclear helium reactions, this happens at $\rho \sim 3 \times 10^{10}$ g cm^{-3}. Since beta decay of the daughter nucleus ^{16}N is prohibited due to complete filling of the electron phase space at $T = 0$, the daughter nucleus immediately undergoes a second electron capture to ^{16}C, as the required density is less than for ^{16}O. At the density required for the double electron capture on ^{16}O, the underlying materials, ^{56}Fe and ^{62}Ni, have already undergone double electron capture to ^{56}Cr, followed by ^{56}Ti, and ^{62}Fe, respectively (see below). As shown in reference [189], this leads to several unstable situations, where a denser layer (i.e. ^{16}C) rests on less dense layers (i.e. ^{56}Ti or ^{62}Fe), resulting in an overturn of the unstable interfaces. This scenario had been proposed as a possible explanation for gamma-ray bursts before these were identified as extra-galactic events with luminosities larger than those observed for supernovae [198].

Double electron capture is expected also to occur in the crust of an accreting neutron star in a binary system. When accretion pushes the original surface layer, made mainly of ^{56}Fe, to higher densities, electron capture will transform ^{56}Fe to ^{56}Cr once $\rho > 1.5 \times 10^{9}$ g cm^{-3}. Haensel and Zdunik studied the consequences for the accreted neutron star crust, built on a single-nucleus (^{56}Fe) approach [7] (see also [199, 200]). Upon pushing the matter to even higher densities, further double electron captures occurred (^{56}Cr $\rightarrow$ ^{56}Ti at $\rho = 1.1 \times 10^{10}$ g cm^{-3}, ^{56}Ti $\rightarrow$ ^{56}Ca at $\rho = 8 \times 10^{10}$ g cm^{-3}, and ^{56}Ca $\rightarrow$ ^{56}Ar at $\rho = 2.5 \times 10^{11}$ g cm^{-3}), before the density was reached at which neutrons are emitted from the nucleus ($\rho = 4.1 \times 10^{11}$ g cm^{-3}, neutron drip). Thus, the double electron capture of ^{56}Ar is accompanied by the emission of free neutrons, ^{56}Ar $\rightarrow$ ^{52}S + 4n. The successive electron captures lower the charge of the nuclei so that pycnonuclear fusion reactions induced by zero-point motion fluctuations in the Coulomb lattice become possible. Double electron captures, and, in particular, pycnonuclear fusion reactions, are a considerable heat source, as discussed in [7, 201].

The crust's composition, which includes nuclei other than ^{56}Fe, complicates the situation. This is also true for the ashes of x-ray burst events which, due to repeating outbursts, are also successively pushed to higher densities and run through a similar sequence to the one described above, of double electron capture, neutron liberation, and pycnonuclear fusion [203]. As pointed out by Schatz *et al* [8], the ashes of former burst events have finite temperatures (a few 10^{8} K) which, although small compared to typical electron capture Q values, open up a small energy window, within which, beta decays of electron capture daughters can occur. For such an URCA process to occur, the electron capture process has to satisfy two conditions: it must be mediated by an allowed transition to a state at excitation energies $E_x < T$ and the beta-decaying nucleus must not have a strong electron capture branch. On general grounds, even–even nuclei, which are the most abundant nuclei in the crust, do not form URCA pairs but rather perform double electron capture [202]. On the other hand, nearly all odd–A nuclei can form URCA pairs. The authors of reference [202] have identified about 85 URCA pairs. Figure 25 shows the neutrino luminosities of these pairs (setting the mass fraction of the nucleus on which an electron is captured to $X = 1$) and the depth in the neutron star at which they operate. As pointed out in [8], cooling by URCA pairs in the crust reduces the heat transport from the crust into the region of the x-ray burst or superburst ashes which reside in the less dense regions (this region is often called the ocean). This lowers the steady-state temperature in the ocean. This puts

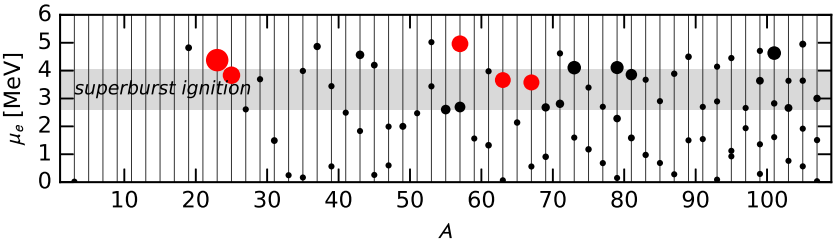

Figure 25. The depths at which URCA pairs of mass number A operate in neutron stars. The size of the data points corresponds to the neutrino luminosity of the pair, setting its mass fraction to $X = 1$. (The top five are colored in red.) The gray band indicates constraints for superburst ignition, assuming an ignition at a column depth between $0.5–3 \times 10^{12}$ g cm^{-2}. Reproduced from [202].

constrains on the ignition of the ^{12}C+^{12}C fusion reaction to start the next burst cycle. This ignition now has to occur at higher densities [202]. URCA pairs can also operate directly in the ocean. However, due to the lower densities, nuclei are less neutron-rich, with smaller Q values for electron capture than those in the crust. Since the neutrino luminosity scales with Q^5, this strongly reduces the effectiveness of URCA pairs in the ocean [202].

Due to the simultaneous observation of the gravitational wave and the electromagnetic signal from GW170817, the merger of two neutron stars in a binary system has been identified as one of the astrophysical sites, see e.g., [204], where the rapid neutron-capture process (r-process) [205–208] operates. The Y_e value of the ejected material, which is determined by weak processes, is particularly important for determining nucleosynthesis in mergers. The initial Y_e profile of the neutron stars can be determined from beta-equilibrium. However, as the neutron stars approach each other and finally merge, the temperature increases and neutrino emission becomes very important. An accurate prediction of the neutrino luminosities requires a description of high density neutrino–matter interactions [209] and its implementation in neutrino radiation transport, as is currently done in core-collapse supernova [210]. The absorption of both ν_e and $\bar{\nu}_e$ together with electron and positron capture leads to substantial changes in the Y_e of the ejected material, particularly in the polar regions [211–214]. These processes occur when the material is hot and is composed mainly of neutrons and protons.

Another important source of material is the so-called secular ejecta originating from the accretion disk that surrounds the central remnant produced by the merger. If this is a long-lived neutron star, the neutrino luminosities are large enough to affect the neutron-to-proton ratio of the ejected material [215]. If the central object is a black hole, the neutron-to-proton ratio is determined by a dynamic beta equilibrium [216] between electron and positron capture and beta-decay operating in the accretion disk [217–220] on hot material that mainly is made of neutrons and protons. According to current understanding, electron capture on nuclei does not play an important role in r-process nucleosynthesis in neutron-star merger events.

4.4. The fate of intermediate-mass stars

The final fates of stars depend on their masses at birth. Stars with masses of less than about $8M_\odot$ advance through hydrogen and helium burning. As they suffer significant mass loss due to stellar winds, their masses at the end of helium burning are not sufficient to ignite further burning stages. They end their lives as WDs. Stars with masses in excess of about $11M_\odot$ develop a core at the end of each burning phase which exceeds the Chandrasekhar mass. As a result, they can ignite the full cycle of hydrostatic burning and end their lives as collapsed-core supernovae, leaving either neutron stars or black holes as remnants. The fate of intermediate-mass stars ($8–11M_\odot$) balances on a knife edge between collapsing into a neutron star or ending in a thermonuclear runaway which disrupts most of the core [221]. Simulations of such stars are quite sensitive to astrophysical uncertainties such as convective mixing or mass loss rates [221]. On the other hand, the major nuclear uncertainty, related to electron capture on ^{20}Ne, has recently been removed, since this rate, as we described in section 3.1.2, is now known experimentally for the relevant astrophysical conditions. We briefly summarize the consequences which this nuclear milestone has for the fate of intermediate-mass stars.

Intermediate-mass stars go through hydrostatic hydrogen, helium and core carbon burning, but are not massive enough to ignite further advanced burning stages. In the center of the star, a core develops which consists mainly of ^{16}O and ^{20}Ne, with smaller amounts of ^{23}Na and ^{24,25}Mg. Due to their position on the Hertzsprung–Russell diagram, stars with such an ONe core are referred to as super AGB stars. It is important to note that the cores of super-AGB stars are denser than their counterparts after helium burning in more massive stars. As nuclear burning has ceased in the ONe core, its gravitational collapse is counteracted by the electron degeneracy pressure. However, the densities achieved in the core result in electron chemical potentials large enough to initiate electron capture reactions, which reduce the pressure withstanding collapse. Here, two distinct processes play an essential role in the development of the core. This is shown in figure 26, which displays the final temperature–density evolution of the core center. First, several URCA pairs (^{25}Mg–^{25}Na, ^{23}Na–^{23}Ne, ^{25}Na–^{25}Ne) operate at various phases of this final evolution. These pairs provide an efficient cooling mechanism. Second, electron captures also occur on the abundant α-nuclei ^{24}Mg and ^{20}Ne once the electron chemical potential overcomes the capture Q values (the Q value of ^{16}O is too high for electron capture at these densities). However, for these $N = Z$ nuclei, the electron capture daughters, (^{24}Na and ^{20}F), also capture electrons which, due to their smaller Q values than the first captures, occur

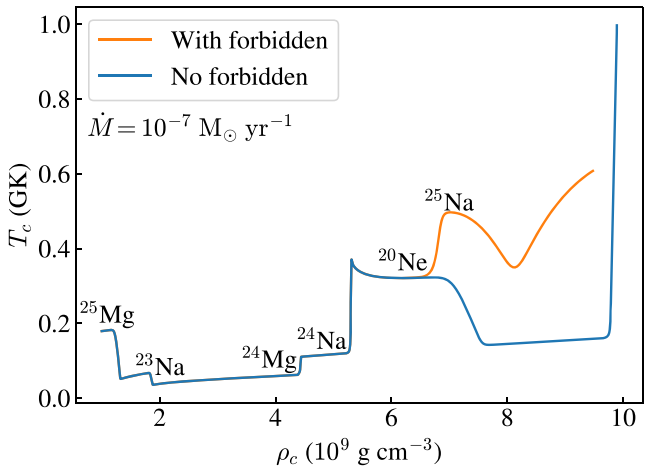

Figure 26. Temperature–density evolution of the ONeMg core of an intermediate-mass star. The labels indicate at which densities the URCA pairs and the electron captures on ^{24}Mg and ^{20}Ne operate. The red (blue) lines show the evolution with (without) inclusion of the forbidden ground-state-to-ground-state contribution to the ^{20}Ne electron capture rate. The calculation assumes that the ONe core accretes a mass of $10^{-7}M_\odot$ per year from ongoing hydrostatic burning. Reprinted figure with permission from [52], Copyright (2019) by the American Physical Society.

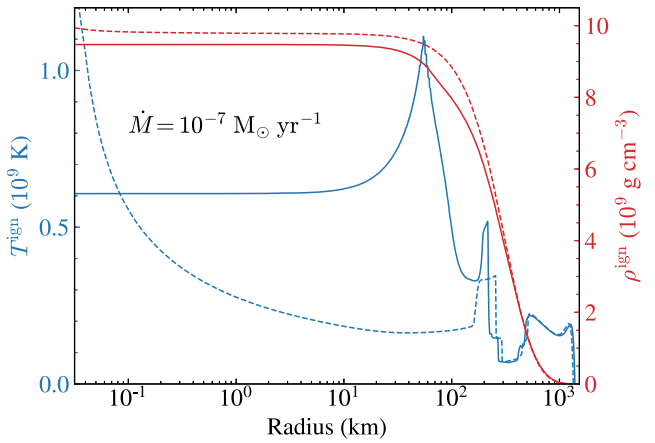

Figure 27. Temperature (blue) and density (red) profiles of an ONe core at the ignition of oxygen fusion, calculated with (solid lines) and without (dashed lines) consideration of the forbidden ground-state-to-ground-state transition in the ^{20}Ne electron capture rate. The calculations were performed using the spherically symmetric MESA code [223], assuming that the ONe core accretes a mass of $10^{-7}M_\odot$ per year from ongoing hydrostatic burning. Reprinted figure with permission from [52], Copyright (2019) by the American Physical Society.

significantly faster than competing β-decays. Furthermore, the second capture often proceeds to excited states in their daughters, which then decay by γ emission to the ground states and heat the environment (see figure 26). Due to its lower initial Q-value, double electron capture on ^{24}Mg proceeds at lower densities than that on ^{20}Ne. Recognizing the low temperature at the onset of electron capture on ^{20}Ne (about 300 keV), largely due to the efficient URCA cooling [222], the authors of reference [51] pointed out that the transition from the ^{20}Ne 0^+ ground state to the ^{20}F 2^+ ground state, although second forbidden, could dominate the rate at core conditions, since all other transitions were exponentially suppressed, either by the tail of the electron distribution, or a Boltzmann factor due to thermal excitation.

The inclusion of the 'forbidden' ground-state-to-ground-state transition in the electron capture rate on ^{20}Ne shifts the onset of this capture to lower densities before the last epoch of URCA cooling by the ^{25}Na–^{25}Ne pair (see figure 26). This shift in density has, however, an important impact on the fate of the star, which ends either in gravitational collapse or thermonuclear explosion. This fate is determined by the competition between electron capture and nuclear energy generation by oxygen fusion [221]. If the ignition of oxygen (requiring temperatures in excess of 10^9 K) occurs at low enough densities, the fusion generates sufficient energy to reverse the collapse and to disrupt the star in a thermonuclear explosion. At higher densities, the deleptonization behind the burning front is so rapid that the loss of pressure cannot be recovered by nuclear burning. In this case, the core continues to collapse, ending as a neutron star. The increase of the ^{20}Ne electron capture rate due to the contribution of the forbidden transition seems to shift the fate toward thermonuclear explosion [52]. This is demonstrated in figure 27, which is based on a spherically symmetric simulation of the core evolution performed with the MESA code [223]. In the calculation performed without the addition of the forbidden contribution to the rate, oxygen is ignited in the center, while in the case that uses the experimental ^{20}Ne capture rate and includes the forbidden transition, the star develops an isothermal core at temperatures below the ignition value. In this inner core, double electron capture on ^{20}Ne continues to generate heat, which leads to an off-center ignition of oxygen burning (at a radius of 58 km for the case shown in figure 27). We also note that, without the forbidden contribution, the core reaches a higher density at ignition.

To determine the fate of the star requires us to study the propagation of the burning front, which needs a 3D hydrodynamic treatment to resolve the relevant length scales. Such studies have been reported in [52] and all simulations matched to the parameters of the spherically symmetric MESA results ended in thermonuclear explosions producing an ONeFe WD remnant. This has significant implications for the total nucleosynthesis yields of intermediate-mass stars, since thermonuclear explosions eject about $0.01M_\odot$ more mass than gravitational collapse and intermediate-mass stars are much more abundant than heavier stars. A first exploration shows that the ejecta of thermonuclear explosions are particularly rich in certain neutron-rich Ca, Ti, and Cr isotopes and in the trans-iron elements Zn, Se, and Kr [52]. This might have interesting implications for the understanding of the early chemical evolution of our Galaxy [224].

4.5. Helium flashes in accreting helium WDs

Subluminous B stars are stars with burning helium cores, thin hydrogen envelopes, and masses of about $0.5M_\odot$ [225]. Often, these stars exist in tight binaries with WDs [226]. When the

WD accretes matter from the unburned outer layers of its companion star, an amount of ^{14}N, a product of hydrogen burning in the CNO cycle, is also present, depending on the initial metallicity of the donor star. Electron capture on ^{14}N is then a decisive factor for the fate of the accreted material.

Due to its low Q value of 0.667 MeV, electrons are captured on ^{14}N once the density of the accreted matter on the WD surface exceeds a threshold value of about 1.156×10^6 g cm^{-3} [227]. As the relevant temperatures are rather low (T less than a few 10^8 K), the capture proceeds solely by the allowed transition between the ^{14}N and ^{14}C ground states. The respective transition matrix element is known from the ^{14}C beta decay. Coulomb corrections due to environmental effects are relatively minor, but are considered in recent astrophysical applications [227].

For the temperatures involved and for densities larger than about 10^6 g cm^{-3}, the electron capture rate is larger than the competing β decay and, in the helium-rich environment, the electron capture is followed by an α capture on ^{14}C [228]. The energy generated by this so-called NCO reaction ($^{14}\mathrm{N}(e^-,\nu_e)^{14}\mathrm{C}(\alpha,\gamma)^{18}\mathrm{O}$) [229]—despite some uncertainties in the α-capture rate on ^{14}C [230]—is larger than that of the triple-alpha reaction in the relevant temperature–density range. Thus, it is the NCO reaction that triggers a rather steep rise of the temperature in the environment so that, as a second step, the triple-alpha reaction is also ignited. This finally leads to a thermonuclear instability which is observed as a helium flash.

The evolution of these flashes depends crucially on the accretion mass flow [228]. If the mass flow is large ($10^{-8} M_\odot$ year^{-1}), the energy released from the subsequent gravitational contraction leads to heating of the environment, enabling a ^{14}C nucleus to capture an α particle rapidly. The electron capture process controls the NCO reaction sequence and an insignificant amount of ^{14}C is built up. For smaller mass flows ($10^{-9} M_\odot$ year^{-1}), the gravitational energy released by core contraction can be radiated away, keeping the temperature in the core low. Hence, when the core density exceeds the value for electron capture, the temperature is too low to ignite α captures on ^{14}C. This occurs at conditions with higher densities and after ^{14}N has been completely converted to ^{14}C. Simulations also show that for smaller accretion rates, the core becomes convectively unstable. The timescale on which the flashes develop also depends on the accretion rate and is significantly shorter for smaller rates (a few 10^7 year for $10^{-9} M_\odot$ year^{-1}).

5. Summary

In his authoritative review of core-collapse supernovae, Hans Bethe stated in 1990 [1]: 'the theory of electron capture has gone a full circle and a half.' He was referring to the fact that in early models, capture was assumed to occur on free protons. This was questioned by BBAL [2], who noted that the concentration of free protons during collapse was very low and that the capture took place on nuclei with mass numbers $A = 60$–80, changing a proton in the $f_{7/2}$ shell to a neutron in the $f_{5/2}$ orbital by an allowed GT transition. Following Bethe, the third semi-circle is due to Fuller's observation that the neutron $f_{5/2}$ orbitals are occupied at neutron number $N = 38$ [17], blocking GT transitions within the pf shell. Hence, at the time when Bethe wrote his famous article, electron capture in supernovae was assumed to occur on free protons and capture on nuclei was switched off for nuclei with $N > 38$ [18].

As we have summarized in this manuscript, the experimental and theoretical work of the last two decades implies that this picture was too simple. Experimental techniques for measuring GT strength distributions based on charge-exchange reactions with progressively better energy resolutions—advancing from the pioneering (n, p) reactions to the much more refined (d,^{2} He) and (t,^{3} He) reactions—have provided clear evidence that nuclear correlations play a decisive role in the total strength, and even more, in the fragmentation of the GT distribution, thus invalidating the IPM on which the early electron capture work, which was discussed and reviewed by Bethe in 1990 [1], was based. In parallel, many-body models became available which were able to account for the relevant nuclear correlations and describe the experimental GT data quite well. Importantly, these models, and also the experimental data, imply that the GT strength is not blocked at the shell gap between the pf and $g_{9/2}$ orbitals caused by strong nuclear cross-shell correlations. As a major consequence, electron capture takes place on nuclei during the entire collapse. With this result, the theory of electron capture has now made two complete circles.

The evaluation of stellar electron capture for core-collapse supernovae rests on the fact that, with progressing core density, the electron chemical potential grows significantly faster than the average Q value which dominate the core composition. As a consequence, detailed descriptions of the nuclear strength functions (i.e. GT) are only needed for nuclei in the Fe–Ni mass range ($A = 45$–65), which are most abundant during the early collapse phase, while for the neutron-rich, heavy nuclei, which dominate later in the collapse at higher densities, a more general reproduction of the strength functions (now, however, including forbidden transitions) will suffice. This is quite a fortunate situation.

For those nuclei for which the calculation of stellar capture rates requires detailed descriptions of the allowed strength functions (pf - and sd-shell nuclei, where the latter occur in the burning stages prior to collapse), diagonalization shell-model calculations can be performed that, in general, reproduce the measured GT strength functions quite well. In fact, if the capture rates are calculated solely from the ground-state distributions, the rates obtained from data and from the shell model agree to within better than a factor of 2 under the relevant astrophysical conditions. The theoretical capture rates (i.e. [13, 34]) consider excited states determined from shell-model calculations, accounting for the fact that each nuclear state has its own individual strength distribution. There are no indications that the shell-model results for excited states might be less reliable than for the ground states. However, there is a concern that the procedure applied in [34] might slightly underestimate the partition function at higher temperatures [138].

The fact that cross-shell correlations unblock GT transitions, even in the ground states of nuclei with proton numbers $Z < 40$ and neutron numbers $N > 40$, has been proven by experimental data for GT strength distributions and also from spectroscopic information obtained from transfer reactions. Thus, the assumption that GT transitions are Pauli blocked for nuclei with $N > 38$ has been disproven by experiment. Modern many-body models, such as the diagonalization shell model (for selected nuclei) and the SMMC approach, can reproduce such cross-shell correlations. The latter approach has been adopted to determine partial occupation numbers in large model spaces, including the shell gaps at $N = 40$ and 50. The capture rates were then calculated within a hybrid model (HM) from these occupation numbers within the framework of the RPA, exploiting the fact that these heavier nuclei become abundant during the collapse at sufficiently high densities, requiring only the overall strength, but not a detailed reproduction of the GT strength functions. The contributions from forbidden transitions were included, which become progressively more important with increasing density. The HM indicates that the gaps at $N = 40$ and 50 lead to some reduction of the capture rates, but the rates are obviously large enough at the relevant temperatures that captures on nuclei dominate those on free protons during the entire collapse. This is clearly borne out in modern supernova simulations, thus closing the second circle referred to by Hans Bethe.

The unblocking of the GT strength at the neutron numbers $N = 40$ and 50 has also been confirmed by calculations performed within the thermal quasiparticle RPA approach, which consistently considers correlations up to the 2p–2h level. As cross-shell correlations in general require configurations beyond 2p–2h, GT strength, in particular at low excitation energies, can be missed. This translates into the observation that, at modest temperatures and densities, capture rates obtained within the TQRPA are somewhat smaller than in the HM. At higher temperatures and densities, the two models give very similar results, including the neutron-rich nuclei with $N = 50$, which significantly contribute to the capture process under these astrophysical conditions. Both theoretical approaches imply that at the respective temperatures of the order of $T = 1$ MeV, configurations from higher shells, which are strongly reduced in the ground state, are present in the thermally excited nuclear states and significantly unblock the GT strength. This observation is quite important, since the ground-state GT distribution for such nuclei has been experimentally observed to have nearly vanishing strength and the electron capture rate would nearly be blocked if calculated from the ground-state distribution. While the unblocking appears to be quite solid on theoretical ground, experimental verification is desirable.

Although core-collapse supernovae are arguably the most important astrophysical application, electron capture also plays a role in other astrophysical environments. In thermonuclear supernovae, the rate of electron capture on nuclei determines the production yield of neutron-rich nuclei. As the relevant nuclei are those in the Fe–Ni mass range, experimental and theoretical (by diagonalization shell-model calculations) progress has constrained the relevant capture rates significantly, to the point where an improved description of the details of the GT strength distribution only changed the nucleosynthesis yields by a few percent. The description of capture rates for *sd*-shell nuclei, again based on shell-model calculations and data, has reached a similar degree of accuracy, which appears to be sufficient for the simulation of this process for the core evolution of intermediate-mass stars. However, attention has recently been drawn to the fact that in the low-temperature–low-density environment of such stellar cores, only a few transitions dominate the capture rates and also that in exceptional situations a forbidden transition can noticeably contribute to the rate. Such a situation happens for the capture on ^{20}Ne, where the second forbidden transition from the ^{20}Ne ground-state to the ^{20}F ground state enhances the capture rate just at the most crucial conditions for the core evolution. The transition strength has now been measured so that the entire electron capture rate on ^{20}Ne is now experimentally determined in the relevant temperature–density regime.

Double electron captures, initiated on abundant even–even nuclei, are relevant for the crust evolution of accreting neutron stars. The process is triggered once the electron chemical potential (i.e. the crustal density) is high enough for electrons to overcome the Q value between the even–even mother nucleus and the odd–odd daughter. As the Q value of the second capture step on the odd–odd nucleus is smaller, due to nuclear pairing, this energy gain can be transferred into heating of the crust. For simulations of the crust's evolution, one is generally not so interested in the capture rate (which is often faster than competing timescales), but in the portion of the energy gain which is translated into heat. As this can involve quite exotic neutron-rich nuclei, a detailed determination of this energy portion is a formidable nuclear-structure challenge and current models are likely to be too uncertain.

Despite the progress that has been achieved in recent years in the determination of stellar electron capture rates, further improvements are certainly desirable and, in specific cases, needed. Additional precision measurements of GT strength distributions for *sd*- and *pf*-shell nuclei will lead to further improvements and to refinements of the shell-model calculations, however, it is not expected that these improvements will have a significant impact on supernova dynamics or nucleosynthesis. It is, however, desirable that the gap of nuclei (with mass numbers $A = 38$–45), for which no shell-model electron capture rates exist, should be filled. Such calculations are challenging, as they require an accurate description of cross-shell correlations. They would certainly benefit from some detailed experimental GT distribution measurements. A particularly interesting and important case is ^{40}Ar, which serves as a material for neutrino detectors such as ICARUS [231–233], which has the potential to detect supernova neutrinos. Detailed GT$_-$ data from (p, n) [234] and (^{3}He, t) charge-exchange data [235] and M1 data from (γ, γ') photon scattering reactions [236] can serve as experimental constraints for the determination of charged-current (ν_e, e^-) and neutral-current (ν, ν') cross-sections on ^{40}Ar. However, GT$_+$ data, which are relevant for electron capture and charged-current $(\bar{\nu}_e, e^+)$ cross-sections do not exist yet. In principle, forbidden transitions, which are not

considered in the shell-model electron capture rates for *sd* and *pf* -shell nuclei, can contribute to the rates. However, such contributions will only be relevant in core-collapse supernovae at higher temperatures than those at which these nuclei dominate the core composition. The cases of ^{20}Ne [52,146] and ^{24}Na [237], for which a second forbidden transition dominates the capture rate at the relevant conditions during the core evolution of intermediate-mass stars, show, however, that such exceptional cases can occur at rather low temperatures, where only a few transitions contribute to the capture rate.

The shell gaps at neutron numbers $N = 40$ and 50 do not block electron capture on nuclei in current supernova models. In both cases, this is based on modern many-body models, which at $N = 40$ overcome the gap by nucleon correlations, while for $N = 50$, thermal excitation is the main unblocking mechanism (plus contributions from other multipoles than GT). For $N = 40$, the finding is supported by experimental data, although it is quite limited so far. It would be desirable to enlarge the data pool. It is particularly tempting that recent developments open up the measurements of GT distributions for unstable neutron-rich nuclei, based on charge-exchange reactions performed in inverse kinematics. Such additional data would certainly be welcome, in order to further constrain models. At $N = 50$, theoretical models imply that cross-shell correlations induced by thermal excitation render ground-state GT distributions inapplicable to the calculation of capture rates at the finite temperatures which exist in the astrophysical environment when these heavier and very neutron-rich nuclei dominate the capture process. Although the two models which have been applied to $N = 50$ nuclei agree rather well in their rate predictions, improvements to the models are conceivable. On one hand, the finite-temperature QRPA model should be extended to non-spherical nuclei and, in the midterm, should also include higher correlations, as in the second QRPA approach. On the other hand, the SMMC approach is uniquely suited to studying nuclear properties at the finite temperatures of relevance. It might be interesting to calculate the GT strength function at those temperatures directly within the SMMC approach. This presupposes the handling of a numerically ill-defined inverse Laplace transformation. First steps in this direction have been taken in reference [238].

Of course, it is always conceivable that future observations or simulations of supernovae or other astrophysical objects will point to the need for particular electron capture rates, which will then require specific experimental and theoretical attention.

In summary, the description of stellar electron capture has come a long and winding way. The experimental and theoretical progress of recent years has probably firmly established that electron capture proceeds on nuclei during core-collapse supernovae. The circle, as referred to by Hans Bethe, might have come to an end.

Acknowledgments

The authors gratefully acknowledge the support and assistance of their colleagues Sam M Austin, B A Brown, E Caurier, S Couch, D J Dean, J Engel, T Fischer, Y Fujita, A Heger, H-T Janka, A Juodagalvis, W R Hix, E Kolbe, O Kirsebom, A Mezzacappa, F Nowacki, E O'Connor, A Poves, J Sampaio, H Schatz, A Spyrou, T Suzuki, F-K Thielemann, S E Woosley, Y Zhi, and A P Zuker. GMP acknowledges the support of the Deutsche Forschungsgemeinschaft (DFG, German Research Foundation)—Project-ID 279384907—SFB 1245 'Nuclei: from fundamental interactions to structure and stars', the European Research Council (ERC) under the European Union's Horizon 2020 research and innovation program (ERC Advanced Grant KILONOVA No. 885281), the Helmholtz Forschungsakademie Hessen für FAIR, and the 'ChETEC' COST Action (CA16117) funded by COST (European Cooperation in Science and Technology). RZ gratefully acknowledges support by the US National Science Foundation under Grants PHY-1913554 (Windows on the Universe: Nuclear Astrophysics at the NSCL), PHY-1430152 (JINA Center for the Evolution of the Elements). KL, GMP and RZ acknowledge support by the National Science Foundation under Grant No. OISE-1927130 (IReNA).

Data availability statement

No new data were created or analysed in this study.

ORCID iDs

G Martínez-Pinedo https://orcid.org/0000-0002-3825-0131
R G T Zegers https://orcid.org/0000-0001-6076-5898

References

[1] Bethe H A 1990 *Rev. Mod. Phys.* **62** 801–66
[2] Bethe H A, Brown G E, Applegate J and Lattimer J M 1979 *Nucl. Phys.* A **324** 487–533
[3] Fuller G M, Fowler W A and Newman M J 1982 *Astrophys. J. Suppl.* **48** 279
[4] Janka H, Langanke K, Marek A, Martínez-Pinedo G and Müller B 2007 *Phys. Rep.* **442** 38–74
[5] Doherty C L, Gil-Pons P, Siess L and Lattanzio J C 2017 *Publ. Astron. Soc. Aust.* **34** e056
[6] Nomoto K and Leung S C 2017 Electron capture supernovae from super asymptotic giant branch stars *Handbook of Supernovae* A Alsabti and P Murdin (Cham: Springer) https://doi.org/10.1007/978-3-319-20794-0_118-1
[7] Haensel P and Zdunik J L 1990 *Astron. Astrophys.* **227** 431
[8] Schatz H *et al* 2014 *Nature* **505** 62–5
[9] Iwamoto K, Brachwitz F, Nomoto K, Kishimoto N, Umeda H, Hix W R and Thielemann F K 1999 *Astrophys. J. Suppl.* **125** 439–62
[10] Brachwitz F *et al* 2000 *Astrophys. J.* **536** 934–47
[11] Cooperstein J and Wambach J 1984 *Nucl. Phys.* A **420** 591–620
[12] Langanke K and Martínez-Pinedo G 2000 *Nucl. Phys.* A **673** 481–508
[13] Juodagalvis A, Langanke K, Hix W R, Martínez-Pinedo G and Sampaio J M 2010 *Nucl. Phys.* A **848** 454–78
[14] Fuller G M, Fowler W A and Newman M J 1980 *Astrophys. J. Suppl.* **42** 447–73

[15] Fuller G M, Fowler W A and Newman M J 1982 *Astrophys. J.* **252** 715
[16] Fuller G M, Fowler W A and Newman M J 1985 *Astrophys. J.* **293** 1
[17] Fuller G M 1982 *Astrophys. J.* **252** 741–64
[18] Bruenn S W 1985 *Astrophys. J. Suppl.* **58** 771–841
[19] Gaarde C *et al* 1981 *Nucl. Phys.* A **369** 258
[20] Osterfeld F 1992 *Rev. Mod. Phys.* **64** 491–557
[21] Vetterli M C *et al* 1990 *Phys. Rev.* C **40** 559–69
[22] Vetterli M C *et al* 1992 *Phys. Rev.* C **45** 997–1004
[23] Helmer R L *et al* 1997 *Phys. Rev.* C **55** 2802
[24] Frekers D 2006 *Prog. Part. Nucl. Phys.* **57** 217–25
[25] Martínez-Pinedo G, Liebendörfer M and Frekers D 2006 *Nucl. Phys.* A **777** 395–423
[26] Frekers D and Alanssari M 2018 *Eur. Phys. J.* A **54** 177
[27] Zegers R G T *et al* 2006 *Phys. Rev.* C **74** 024309
[28] Langanke K and Martínez-Pinedo G 2003 *Rev. Mod. Phys.* **75** 819–62
[29] Heger A, Woosley S E, Martinez-Pinedo G and Langanke K 2001 *Astrophys. J.* **560** 307–25
[30] Caurier E, Martínez-Pinedo G, Nowacki F, Poves A and Zuker A P 2005 *Rev. Mod. Phys.* **77** 427–88
[31] Brown B A and Wildenthal B H 1988 *Annu. Rev. Nucl. Part. Sci.* **38** 29–66
[32] Caurier E, Langanke K, Martínez-Pinedo G and Nowacki F 1999 *Nucl. Phys.* A **653** 439–52
[33] Oda T, Hino M, Muto K, Takahara M and Sato K 1994 *At. Data Nucl. Data Tables* **56** 231–403
[34] Langanke K and Martínez-Pinedo G 2001 *At. Data Nucl. Data Tables* **79** 1–46
[35] Heger A, Langanke K, Martínez-Pinedo G and Woosley S E 2001 *Phys. Rev. Lett.* **86** 1678–81
[36] Langanke K, Kolbe E and Dean D J 2001 *Phys. Rev.* C **63** 032801
[37] Zhi Q, Caurier E, Cuenca-García J J, Langanke K, Martínez-Pinedo G and Sieja K 2013 *Phys. Rev.* C **87** 025803
[38] Grewe E W *et al* 2008 *Phys. Rev.* C **78** 044301
[39] Langanke K *et al* 2003 *Phys. Rev. Lett.* **90** 241102
[40] Johnson C W, Koonin S E, Lang G H and Ormand W E 1992 *Phys. Rev. Lett.* **69** 3157–60
[41] Koonin S E, Dean D J and Langanke K 1997 *Phys. Rep.* **278** 1–77
[42] Hix W R, Messer O E B, Mezzacappa A, Liebendörfer M, Sampaio J, Langanke K, Dean D J and Martínez-Pinedo G 2003 *Phys. Rev. Lett.* **91** 201102
[43] Hix W R and Thielemann F-K 1996 *Astrophys. J.* **460** 869–94
[44] Dzhioev A A, Vdovin A I, Ponomarev V Y, Wambach J, Langanke K and Martínez-Pinedo G 2010 *Phys. Rev.* C **81** 015804
[45] Dzhioev A A, Langanke K, Martínez-Pinedo G, Vdovin A I and Stoyanov C 2020 *Phys. Rev.* C **101** 025805
[46] Nomoto K 1987 *Astrophys. J.* **322** 206–14
[47] Takahara M, Hino M, Oda T, Muto K, Wolters A A, Glaudemans P W M and Sato K 1989 *Nucl. Phys.* A **504** 167–92
[48] Parikh A, José J, Seitenzahl I R and Röpke F K 2013 *Astron. Astrophys.* **557** A3
[49] Bravo E 2019 *Astron. Astrophys.* **624** A139
[50] Suzuki T, Toki H and Nomoto K 2016 *Astrophys. J.* **817** 163
[51] Martínez-Pinedo G, Lam Y H, Langanke K, Zegers R G T and Sullivan C 2014 *Phys. Rev.* C **89** 045806
[52] Kirsebom O S *et al* 2019 *Phys. Rev. Lett.* **123** 262701
[53] Bahcall J N 1962 *Phys. Rev.* **128** 1297–301
[54] Bahcall J N and Moeller C P 1969 *Astrophys. J.* **155** 511
[55] Johnson C W, Kolbe E, Koonin S E and Langanke K 1992 *Astrophys. J.* **392** 320–7
[56] Adelberger E G *et al* 1998 *Rev. Mod. Phys.* **70** 1265–91
[57] Adelberger E G *et al* 2011 *Rev. Mod. Phys.* **83** 195–245
[58] Simonucci S, Taioli S, Palmerini S and Busso M 2013 *Astrophys. J.* **764** 118
[59] Clayton D D 1968 *Principles of Stellar Evolution and Nucleosynthesis* (New York: McGraw-Hill)
[60] Takahashi K and Yokoi K 1983 *Nucl. Phys.* A **404** 578–98
[61] Takahashi K and Yokoi K 1987 *At. Data Nucl. Data Tables* **36** 375–409
[62] Yokoi K, Takahashi K and Arnould M 1985 *Astron. Astrophys.* **145** 339–46
[63] Kappeler F, Beer H and Wisshak K 1989 *Rep. Prog. Phys.* **52** 945–1013
[64] Käppeler F, Gallino R, Bisterzo S and Aoki W 2011 *Rev. Mod. Phys.* **83** 157–93
[65] Harakeh M N and van der Woude A 2001 *Giant Resonances: Fundamental High-Frequency Modes of Nuclear Excitations* (New York: Oxford University Press)
[66] Ichimura M, Sakai H and Wakasa T 2006 *Prog. Part. Nucl. Phys.* **56** 446–531
[67] Fujita Y, Rubio B and Gelletly W 2011 *Prog. Part. Nucl. Phys.* **66** 549–606
[68] Taddeucci T N *et al* 1987 *Nucl. Phys.* A **469** 125–72
[69] Ikeda K, Fujii S and Fujita J I 1963 *Phys. Lett.* **3** 271–2
[70] Gaarde C 1985 *Proc. Niels Bohr Centennial Conf. on Nuclear Structure* (Copenhagen) ed R A Broglia, G B Hagemann and B Herskind (Amsterdam: North-Holland) p 449c
[71] Langanke K and Kolbe E 2001 *At. Data Nucl. Data Tables* **79** 293–315
[72] Balasi K G, Langanke K and Martínez-Pinedo G 2015 *Prog. Part. Nucl. Phys.* **85** 33–81
[73] Love W G and Franey M A 1981 *Phys. Rev.* C **24** 1073–94
[74] Sasano M *et al* 2009 *Phys. Rev.* C **79** 024602
[75] Zegers R G T *et al* 2007 *Phys. Rev. Lett.* **99** 202501
[76] Perdikakis G *et al* 2011 *Phys. Rev.* C **83** 054614
[77] Moinester M A *et al* 1989 *Phys. Lett.* B **230** 41–5
[78] Noji S *et al* 2014 *Phys. Rev. Lett.* **112** 252501
[79] Miki K *et al* 2012 *Phys. Rev. Lett.* **108** 262503
[80] Auerbach N 1998 *Comments Nucl. Part. Phys.* **22** 223
[81] Auerbach N, Osterfeld F and Udagawa T 1989 *Phys. Lett.* B **219** 184–8
[82] Hitt G W *et al* 2006 *Nucl. Instrum. Methods Phys. Res.* A **566** 264–9
[83] Helmer R 1987 *Can. J. Phys.* **65** 588
[84] Yen S 1987 *Can. J. Phys.* **65** 595
[85] Alford W P *et al* 1990 *Nucl. Phys.* A **514** 49–65
[86] Alford W P *et al* 1991 *Nucl. Phys.* A **531** 97–111
[87] Alford W P *et al* 1993 *Phys. Rev.* C **48** 2818
[88] Vetterli M C *et al* 1987 *Phys. Rev. Lett.* **59** 439
[89] Vetterli M C *et al* 1989 *Phys. Rev.* C **40** 559
[90] El-Kateb S *et al* 1994 *Phys. Rev.* C **49** 3128–36
[91] Williams A L *et al* 1995 *Phys. Rev.* C **51** 1144–53
[92] Ohnuma H *et al* 1993 *Phys. Rev.* C **47** 648–51
[93] Xu H M, Ajupova G K, Betker A C, Gagliardi C A, Kokenge B, Lui Y-W and Zaruba A F 1995 *Phys. Rev.* C **52** R1161–5
[94] Rakers S *et al* 2002 *Nucl. Instrum. Methods Phys. Res.* A **481** 253–61
[95] Bäumer C *et al* 2003 *Phys. Rev.* C **68** 031303(R)
[96] Rakers S *et al* 2004 *Phys. Rev.* C **70** 054302
[97] Bäumer C *et al* 2005 *Phys. Rev.* C **71** 024603
[98] Hagemann M *et al* 2004 *Phys. Lett.* B **579** 251
[99] Hagemann M *et al* 2005 *Phys. Rev.* C **71** 014606
[100] Popescu L *et al* 2007 *Phys. Rev.* C **75** 054312
[101] Grewe E W *et al* 2008 *Phys. Rev.* C **77** 064303
[102] Guillot J *et al* 2006 *Phys. Rev.* C **73** 014616
[103] Bazin D, Caggiano J A, Sherrill B M, Yurkon J and Zeller A 2003 *Nucl. Instrum. Methods Phys. Res.* B **204** 629
[104] Fujita H *et al* 2002 *Nucl. Instrum. Methods Phys. Res.* A **484** 17–26
[105] Gao B *et al* 2020 *Phys. Rev.* C **101** 014308
[106] Titus R *et al* 2019 *Phys. Rev.* C **100** 045805
[107] Zamora J C *et al* 2019 *Phys. Rev.* C **100** 032801
[108] Noji S *et al* 2015 *Phys. Rev.* C **92** 024312

[109] Scott M *et al* 2014 *Phys. Rev.* C **90** 025801
[110] Hitt G W *et al* 2009 *Phys. Rev.* C **80** 014313
[111] Cole A L *et al* 2006 *Phys. Rev.* C **74** 034333
[112] Paschalis S *et al* 2013 *Nucl. Instrum. Methods Phys. Res.* A **709** 44–55
[113] Bohr A and Mottelson B R 1969 *Nuclear Structure* vol I (New York: Benjamin)
[114] Anantaraman N *et al* 2008 *Phys. Rev.* C **78** 065803
[115] Cole A L, Anderson T S, Zegers R G T, Austin S M, Brown B A, Valdez L, Gupta S, Hitt G W and Fawwaz O 2012 *Phys. Rev.* C **86** 015809
[116] Sasano M *et al* 2011 *Phys. Rev. Lett.* **107** 202501
[117] Sasano M *et al* 2012 *Phys. Rev.* C **86** 034324
[118] Perdikakis G *et al* 2012 *Nucl. Instrum. Methods Phys. Res.* A **686** 117–24
[119] Yasuda J *et al* 2018 *Phys. Rev. Lett.* **121** 132501
[120] Zegers R G T *et al* 2010 *Phys. Rev. Lett.* **104** 212504
[121] Meharchand R *et al* 2012 *Phys. Rev. Lett.* **108** 122501
[122] Ayyad Y *et al* 2020 *Nucl. Instrum. Methods Phys. Res.* A **954** 161341
[123] Hix W R, Mezzacappa A, Messer O E B and Bruenn S W 2003 *J. Phys. G: Nucl. Part. Phys.* **29** 2523–42
[124] Dzhioev A A, Vdovin A I, Wambach J and Ponomarev V Y 2014 *Phys. Rev.* C **89** 035805
[125] Dzhioev A A, Vdovin A I and Wambach J 2015 *Phys. Rev.* C **92** 045804
[126] Langanke K, Dean D J, Radha P B, Alhassid Y and Koonin S E 1995 *Phys. Rev.* C **52** 718–25
[127] Martínez-Pinedo G, Poves A, Caurier E and Zuker A P 1996 *Phys. Rev.* C **53** R2602–5
[128] Caurier E, Poves A and Zuker A P 1995 *Phys. Rev. Lett.* **74** 1517–20
[129] Wakasa T *et al* 1997 *Phys. Rev.* C **55** 2909–22
[130] Gysbers P *et al* 2019 *Nat. Phys.* **15** 428–31
[131] Suzuki T, Honma M, Mao H, Otsuka T and Kajino T 2011 *Phys. Rev.* C **83** 044619
[132] Honma M, Otsuka T, Mizusaki T, Hjorth-Jensen M and Brown B A 2005 *J. Phys.: Conf. Ser.* **20** 002
[133] Poves A, Sánchez-Solano J, Caurier E and Nowacki F 2001 *Nucl. Phys.* A **694** 157–98
[134] Honma M, Otsuka T, Brown B A and Mizusaki T 2002 *Phys. Rev.* C **65** 061301
[135] Brink D M 1955 *PhD Thesis* Oxford University
[136] Axel P 1968 Simple nuclear excitations distributed among closely spaced levels *Proc. on Int. Symp. on Nuclear Structure* (Vienna: IAEA) p 299
[137] Langanke K and Martínez-Pinedo G 1999 *Phys. Lett.* B **453** 187–93
[138] Misch G W, Fuller G M and Brown B A 2014 *Phys. Rev.* C **90** 065808
[139] Tan L, Liu Y-X, Wang L-J, Li Z and Sun Y 2020 *Phys. Lett.* B **805** 135432
[140] Aufderheide M B, Fushiki I, Woosley S E and Hartmann D H 1994 *Astrophys. J. Suppl.* **91** 389–417
[141] Martínez-Pinedo G, Langanke K and Dean D J 2000 *Astrophys. J. Suppl.* **126** 493–9
[142] Wildenthal B H 1984 *Prog. Part. Nucl. Phys.* **11** 5–51
[143] Brown B A and Richter W A 2006 *Phys. Rev.* C **74** 034315
[144] Toki H, Suzuki T, Nomoto K, Jones S and Hirschi R 2013 *Phys. Rev.* C **88** 015806
[145] Anderson B D *et al* 1991 *Phys. Rev.* C **43** 50–8
[146] Kirsebom O S *et al* 2019 *Phys. Rev.* C **100** 065805
[147] Zhi Q, Langanke K, Martínez-Pinedo G, Nowacki F and Sieja K 2011 *Nucl. Phys.* A **859** 172–84
[148] Takahasi Y and Umezawa H 1975 *Collect. Phenom.* **2** 55–80
[149] Dzhioev A A, Vdovin A I and Stoyanov C 2019 *Phys. Rev.* C **100** 025801
[150] Paar N, Colò G, Khan E and Vretenar D 2009 *Phys. Rev.* C **80** 055801
[151] Niu Y F, Paar N, Vretenar D and Meng J 2011 *Phys. Rev.* C **83** 045807
[152] Yako K *et al* 2005 *Phys. Lett.* B **615** 193–9
[153] Pfeiffer A, Mairle G, Knöpfle K T, Kihm T, Seegert G, Grabmayr P, Wagner G J, Bechtold V and Friedrich L 1986 *Nucl. Phys.* A **455** 381–98
[154] Sullivan C, O'Connor E, Zegers R G T, Grubb T and Austin S M 2016 *Astrophys. J.* **816** 44
[155] Pascal A, Giraud S, Fantina A F, Gulminelli F, Novak J, Oertel M and Raduta A R 2020 *Phys. Rev.* C **101** 015803
[156] Raduta A R, Gulminelli F and Oertel M 2017 *Phys. Rev.* C **95** 025805
[157] Nabi J-U and Klapdor-Kleingrothaus H V 1999 *Eur. Phys. J.* A **5** 337–9
[158] Pruet J and Fuller G M 2003 *Astrophys. J. Suppl.* **149** 189–203
[159] Titus R, Sullivan C, Zegers R G T, Brown B A and Gao B 2018 *J. Phys. G: Nucl. Part. Phys.* **45** 014004
[160] Sullivan C, Zegers R G T, Titus R, Brown B A, Gao B, Grubb T O and O'Connor E 2018 Weak rate library https://groups.nscl.msu.edu/charge_exchange/weakrates.html
[161] O'Connor E 2015 *Astrophys. J. Supp.* **219** 24
[162] Koonin S E, Dean D J and Langanke K 1997 *Annu. Rev. Nucl. Part. Sci.* **47** 463–504
[163] Radha P B, Dean D J, Koonin S E, Langanke K and Vogel P 1997 *Phys. Rev.* C **56** 3079–86
[164] Dean D J, Langanke K, Chatterjee L, Radha P B and Strayer M R 1998 *Phys. Rev.* C **58** 536–44
[165] Litvinova E and Robin C 2021 *Phys. Rev.* C **103** 024326
[166] Ravlic A, Yuksel E, Niu Y F and Paar N 2020 arXiv:2010.06394
[167] Woosley S E and Weaver T A 1995 *Astrophys. J. Suppl.* **101** 181
[168] Kotake K, Sumiyoshi K, Yamada S, Takiwaki T, Kuroda T, Suwa Y and Nagakura H 2012 *Prog. Theor. Exp. Phys.* **2012** 01A301
[169] Burrows A 2013 *Rev. Mod. Phys.* **85** 245–61
[170] Janka H-T, Melson T and Summa A 2016 *Annu. Rev. Nucl. Part. Sci.* **66** 341–75
[171] Müller B 2020 *Living Rev. Comput. Astrophys.* **6** 3
[172] Burrows A and Vartanyan D 2021 *Nature* **589** 29–39
[173] Fischer T, Langanke K and Martínez-Pinedo G 2013 *Phys. Rev.* C **88** 065804
[174] Furusawa S 2018 *Phys. Rev.* C **98** 065802
[175] Nagakura H, Furusawa S, Togashi H, Richers S, Sumiyoshi K and Yamada S 2019 *Astrophys. J. Suppl.* **240** 38
[176] Raduta A R, Gulminelli F and Oertel M 2016 *Phys. Rev.* C **93** 025803
[177] Hillebrandt W and Niemeyer J C 2000 *Annu. Rev. Astron. Astrophys.* **38** 191–230
[178] Hillebrandt W, Kromer M, Röpke F K and Ruiter A J 2013 *Front. Phys.* **8** 116–43
[179] Lach F, Röpke F K, Seitenzahl I R, Coté B, Gronow S and Ruiter A J 2020 *Astron. Astrophys.* **644** A118
[180] Nomoto K, Thielemann F-K and Yokoi K 1984 *Astrophys. J.* **286** 644–58
[181] Phillips M M 1993 *Astrophys. J.* **413** L105
[182] Mori K, Famiano M A, Kajino T, Suzuki T, Hidaka J, Honma M, Iwamoto K, Nomoto K and Otsuka T 2016 *Astrophys. J.* **833** 179
[183] Brachwitz F 2001 Neutron-rich nucleosyntheis in Chandrasekhar mass models of type Ia supernovae *PhD Thesis* Universität Basel
[184] Suzuki T 2017 *Mem. Soc. Astron. Ital.* **88** 282
[185] Seitenzahl I R, Cescutti G, Röpke F K, Ruiter A J and Pakmor R 2013 *Astron. Astrophys.* **559** L5
[186] Seitenzahl I R and Townsley D M 2017 Nucleosynthesis in thermonuclear supernovae *Handbook of Supernovae* A Alsati and P Murdin (Cham: Springer) https://doi.org/10.1007/978-3-319-21846-5_87

[187] Piersanti L, Bravo E, Cristallo S, Domínguez I, Straniero O, Tornambé A and Martínez-Pinedo G 2017 *Astrophys. J.* **836** L9
[188] Zegers R G T *et al* 2008 *Phys. Rev.* C **77** 024307
[189] Blaes O, Blandford R, Madau P and Koonin S 1990 *Astrophys. J.* **363** 612
[190] Woosley S E *et al* 2004 *Astrophys. J. Suppl.* **151** 75–102
[191] Galloway D K, Muno M P, Hartman J M, Psaltis D and Chakrabarty D 2008 *Astrophys. J. Suppl. Ser.* **179** 360–422
[192] Keek L, Heger A and in't Zand J J M 2012 *Astrophys. J.* **752** 150
[193] Cameron A G W 1959 *Astrophys. J.* **130** 916
[194] Gasques L R, Afanasjev A V, Beard M, Chamon L C, Ring P and Wiescher M 2005 *Nucl. Phys.* A **758** 134–7
[195] Fushiki I and Lamb D Q 1987 *Astrophys. J.* **323** L55
[196] Schramm S, Langanke K and Koonin S E 1992 *Astrophys. J.* **397** 579
[197] Müller H-M and Langanke K 1994 *Phys. Rev.* C **49** 524–32
[198] Piran T 2005 *Rev. Mod. Phys.* **76** 1143–210
[199] Sato K 1979 *Prog. Theor. Phys.* **62** 957
[200] Bisnovatyi-Kogan G S and Chechetkin V M 1979 *Sov. Phys. - Usp.* **22** 89
[201] Yakovlev D G, Haensel P, Baym G and Pethick C 2013 *Phys.-Usp.* **56** 289–95
[202] Deibel A, Meisel Z, Schatz H, Brown E F and Cumming A 2016 *Astrophys. J.* **831** 13
[203] Schatz H *et al* 1998 *Phys. Rep.* **294** 167–263
[204] Kasen D, Metzger B, Barnes J, Quataert E and Ramirez-Ruiz E 2017 *Nature* **551** 80–4
[205] Burbidge E M, Burbidge G R, Fowler W A and Hoyle F 1957 *Rev. Mod. Phys.* **29** 547–650
[206] Cameron A G W 1957 *Stellar Evolution, Nuclear Astrophysics, and Nucleogenesis Report CRL-41 Chalk River*
[207] Cowan J J, Thielemann F-K and Truran J W 1991 *Phys. Rep.* **208** 267–394
[208] Cowan J J, Sneden C, Lawler J E, Aprahamian A, Wiescher M, Langanke K, Martínez-Pinedo G and Thielemann F K 2021 *Rev. Mod. Phys.* **93** 015002
[209] Burrows A, Reddy S and Thompson T A 2006 *Nucl. Phys.* A **777** 356–94
[210] Janka H T 2017 Neutrino emission from supernovae *Handbook of Supernovae* A Alsabti and P Murdin (Cham: Springer) https://doi.org/10.1007/978-3-319-20794-0_4-1
[211] Wanajo S, Sekiguchi Y, Nishimura N, Kiuchi K, Kyutoku K and Shibata M 2014 *Astrophys. J.* **789** L39
[212] Goriely S, Bauswein A, Just O, Pllumbi E and Janka H-T 2015 *Mon. Not. R. Astron. Soc.* **452** 3894–904
[213] Martin D, Perego A, Kastaun W and Arcones A 2018 *Class. Quantum Grav.* **35** 034001
[214] Radice D, Perego A, Hotokezaka K, Fromm S A, Bernuzzi S and Roberts L F 2018 *Astrophys. J.* **869** 130
[215] Shibata M and Hotokezaka K 2019 *Annu. Rev. Nucl. Part. Sci.* **69** 41–64
[216] Arcones A, Martínez-Pinedo G, Roberts L F and Woosley S E 2010 *Astron. Astrophys.* **522** A25
[217] Beloborodov A M 2003 *Astrophys. J.* **588** 931–44
[218] Siegel D M and Metzger B D 2018 *Astrophys. J.* **858** 52
[219] Fujibayashi S, Shibata M, Wanajo S, Kiuchi K, Kyutoku K and Sekiguchi Y 2020 *Phys. Rev.* D **101** 083029
[220] Just O, Goriely S, Janka H T, Nagataki S and Bauswein A 2021 arXiv:2102.08387
[221] Jones S, Röpke F K, Pakmor R, Seitenzahl I R, Ohlmann S T and Edelmann P V F 2016 *Astron. Astrophys.* **593** A72
[222] Schwab J, Bildsten L and Quataert E 2017 *Mon. Not. R. Astron. Soc.* **472** 3390–406
[223] Paxton B *et al* 2018 *Astrophys. J. Suppl.* **234** 34
[224] Jones S *et al* 2019 *Astron. Astrophys.* **622** A74
[225] Heber U 2009 *Annu. Rev. Astron. Astrophys.* **47** 211–51
[226] Geier S, Østensen R H, Nemeth P, Gentile Fusillo N P, Gänsicke B T, Telting J H, Green E M and Schaffenroth J 2017 *Astron. Astrophys.* **600** A50
[227] Bauer E B, Schwab J and Bildsten L 2017 *Astrophys. J.* **845** 97
[228] Hashimoto M-A, Nomoto K-I, Arai K and Kaminisi K 1986 *Astrophys. J.* **307** 687–93
[229] Kaminisi K, Arai K and Yoshinaga K 1975 *Prog. Theor. Phys.* **53** 1855–6
[230] Iliadis C, Longland R, Champagne A E, Coc A and Fitzgerald R 2010 *Nucl. Phys.* A **841** 31–250
[231] Bueno A, Gil-Botella I and Rubbia A 2003 arXiv:hep-ph/0307222
[232] Gil-Botella I and Rubbia A 2003 *J. Cosmol. Astropart. Phys.* JCAP10(2003)009
[233] Scholberg K 2012 *Annu. Rev. Nucl. Part. Sci.* **62** 81–103
[234] Bhattacharya M, Goodman C D and García A 2009 *Phys. Rev.* C **80** 055501
[235] Karakoç M *et al* 2014 *Phys. Rev.* C **89** 064313
[236] Li T C *et al* 2006 *Phys. Rev.* C **73** 054306
[237] Strömberg D FMartínez-Pinedo GNowacki F 2021 arXiv:2104.02614
[238] Radha P B, Dean D J, Koonin S E, Kuo T T S, Langanke K, Poves A, Retamosa J and Vogel P 1996 *Phys. Rev. Lett.* **76** 2642